Minimalistic mycoplasmas harbor different functional toxin-antitoxin systems

Virginia Hill[1,2], Hatice Akarsu[1], Rubén Sánchez Barbarroja[1], Valentina Cippà[1], Martin Heller[3], Laurent Falquet[4], Manfred Heller[5], Michael H. Stoffel[6], Fabien Labroussaa[1#], Joerg Jores[1#*]

[1] Institute of Veterinary Bacteriology, University of Bern, Bern, Switzerland

[2] Graduate School for Biomedical Science, University of Bern, Bern, Switzerland

[3] Friedrich-Loeffler-Institute - Federal Research Institute for Animal Health, Jena, Germany

[4] Biochemistry Unit, University of Fribourg and Swiss Institute of Bioinformatics, Fribourg, Switzerland

[5] Proteomics and Mass Spectrometry Core Facility, Department for BioMedical Research (DBMR), University of Bern, Bern, Switzerland.

[6] Division of Veterinary Anatomy, University of Bern, Department of Clinical Research and Veterinary Public Health, Switzerland

[#] equal contribution

[*]Corresponding author: Email: joerg.jores@vetsuisse.unibe.ch, Tel.: +41 31 631 2414

Short title: Toxin-antitoxin systems in mycoplasmas

Keywords: *Mycoplasma mycoides* subsp. *capri*; toxin-antitoxin system, TA-system, genome, GM12, cloning

Abstract

Mycoplasmas are minute bacteria controlled by very small genomes ranging from 0.6 to 1.4 Mbp. They lack a cell wall and have been suggested to have progressed through reductive evolution from phylogenetically closely related Clostridia. They are known to colonize the respiratory tract or the urogenital tract among other organs and can cause chronic and subclinical diseases associated with long persistence of the causative agent. Toxin-antitoxin systems (TAS) are genetic elements that have been described for several respiratory and urogenital pathogens as well as for Clostridia, but never for pathogenic mycoplasmas. Here we describe for the first-time different types of TAS in a *Mycoplasma* pathogen, namely *M. mycoides* subsp. *capri*. We identified candidate TAS *in silico* via TASmania database. Two candidate TAS identified *in silico* and another candidate TAS suggested in a minimal cell based on transposon mutagenesis were systematically tested for their functionality in hosts with different phylogenetic distance using heterologous expression. Phylogenetic distance of the host used for heterologous expression influenced the outcome of the functional testing. We corroborated functionality of the three candidate TAS in *Mycoplasma capricolum* subsp. *capricolum*. Moreover, we confirmed transcription and translation of molecules of the TAS investigated during *in vitro* growth. We sequence analyzed 15 genomes of *M. mycoides* subsp. *capri* and revealed an unequal distribution of the TAS studied pointing towards dynamic gain and loss of TAS within the species.

Author summary

Mycoplasmas have a minimal genome and have never been shown to possess TAS. In this work we showed the presence of different functional TAS systems in *Mycoplasma mycoides* subsp. *capri*, a caprine pathogen for the first time. Sequence analysis of a number of *Mycoplasma mycoides* subsp. *capri* strains revealed a plasticity of the genome with respect to TAS carriage. This work paves the way to investigate the biological role of TAS (e.g.

46 persistence, stress tolerance) during infection using mycoplasmas as a simple model organism.
47 Since most mycoplasmas lack classical virulence factors such as exotoxins and go into a kind
48 of stealth mode to evade the immune system, TAS are likely to contribute to the parasitic
49 lifestyle of mycoplasmas and should be investigated in that respect. The availability of
50 synthetic genomics tools to modify a range of *Mycoplasma* pathogens and well-established
51 challenge models for the latter mycoplasmas will foster future research on TAS in
52 mycoplasmas.

Introduction

Mycoplasmas are the smallest bacteria that can replicate in axenic media reported so far. Their cell size and genome size are minute compared to most other bacteria. The genomes range from 0.6 to 1.4 Mbp, a feature that attracted researchers to use mycoplasmas as model organisms for synthetic cells [1] and minimal cells [2]. The small genome size has been attributed to a reductive evolution of mycoplasmas, which are lacking a cell wall and are phylogenetically closely related to spore-forming GRAM-positive bacteria, the Clostridia [3]. A characteristic feature of the mycoplasmas is their parasitic lifestyle, which is reflected by their inability to synthesize essential building blocks of life such as amino acids and hitherto their dependence on a host to provide these building blocks to fuel the anabolic pathways.

Mycoplasmas colonize different niches of their hosts such as mucous membranes of the respiratory tract, the ear canal or the urogenital system. The genus *Mycoplasma* encompasses important human pathogens such as *M. genitalium* [4] and *M. pneumoniae* [5] as well as pathogens of utmost veterinary importance such as *M. mycoides* subsp. *mycoides* [6], *M. capricolum* subsp. *capripneumoniae* [7] and *M. hyopneumoniae* [8]. Although a number of mycoplasmas cause diseases with a relatively short incubation time and high lethality as known for contagious caprine pleuropneumonia [9], many *Mycoplasma* infections are chronic and associated with a long persistence of the causative agent [10, 11].

Toxin-antitoxin systems (TAS) are chromosomal or extrachromosomal genetic elements, which can be grouped into six different types according to their mode of action [12]. All TAS encode a toxin (T), which is able to interfere with vital processes of the bacterial cell related to transcription, translation, replication and membrane integrity, as well as an antitoxin (A) that inhibits the activity of the toxin, so that it cannot interfere with the vital cellular processes. TAS have been described for a wide range of GRAM-positive and GRAM-negative bacteria including pathogens of the gastrointestinal and respiratory tract such as Clostridia and

Mycobacteria, respectively. The role of TAS has been attributed to reduce metabolism during stress, hinder bacteriophages, stabilize genetic elements, and modulate the build-up of biofilms [13].

Pathogenic mycoplasmas are not known for classical exotoxins, the only exception is an ADP-ribosyltransferase (ART) activity-conferring toxin identified in *M. pneumoniae* [14]. So far, TAS have not been documented in mycoplasmas. The presence of a TAS in an engineered strain of *Mycoplasma mycoides* subsp. *capri* (*Mmc*) with a heavily reduced genome has been suggested based on polar effects of transposon insertions [15], but was never confirmed using heterologous expression or shown in its parental wild type strain GM12.

The goal of this study was to shed light on the presence of TAS in mycoplasmas, which are known for their minute genome size. Therefore, we chose *Mmc* GM12, a caprine pathogen [16] used to study virulence traits [17-19] and used as model organism for synthetic genomics. We performed an *in silico* analysis to identify candidate TAS, which were subsequently systematically tested for their functionality in hosts with different phylogenetic distance using heterologous expression. Thereafter, we examined the presence of the candidate TAS at the species and genus level and noticed an unequal distribution pointing towards horizontal gene transfer to be involved in dissemination of the TAS over different mycoplasmas.

Results

Candidate TAS identified *in silico* by TASmania database search

The database TASmania [20], which is a discovery-oriented database, was used here to identify candidate TAS in *Mmc* GM12. Our *in silico* search revealed 38 genes encoding candidate toxins or antitoxins (**Table S1**). With respect to our cut-off settings, the following five genes/gene pairs qualified as candidate TAS: MMCAP1_0160/0161, MMCAP1_0890, MMCAP1_0731, MMCAP1_0525, MMCAP1_0753 (**Table 1**). Four of the latter TAS candidates were without a proposed counterpart, the corresponding toxins or antitoxins were manually chosen using 'guilt by association', considering the cognate loci of the respective gene as the partner of a two gene operon. A transposon library of JCVI-syn2.0, a synthetic mycoplasma cell, controlled by a reduced genome of *Mmc* strain GM12, suggested JCVISYN2_0132 (referred here as A_{132}) and JCVISYN2_0133 (referred to as T_{133}) to act as putative TAS [15]. Therefore, we included this candidate TAS into our study.

The six candidate TAS were distributed throughout the *Mmc* GM12 genome (**Figure 1**). Inspecting the gene loci, we observed that $TAS_{133/2}$ and $TAS_{731/0}$ were arranged in a classical TAS operon structure, with the antitoxin upstream of the toxin and one promotor. $TAS_{525/4}$, $TAS_{160/1}$ and $TAS_{889/0}$ were arranged in a classical operon structure but in antisense orientation. $TAS_{752/3}$ had a non-classical TAS operon structure with the toxin upstream of the antitoxin and an intergenic region of 207 bp. Analysis of this intergenic region using BPROM identified one possible promotor with the putative -10 and -35 boxes, indicating that the antitoxin has its own promotor (**Figure 1**).

Gene description on TASmania database denominated $TAS_{160/1}$ as abortive infection proteins, AbiGII (T_{160}) and AbiGI (A_{161}), which belong to a well-described protein family (Abi), described to act as toxin-antitoxin systems in e.g. *Streptococcus agalactiae* [21]. T_{752} was denominated as cell filamentation protein (fic) and A_{753} as DNA-damage-inducible protein J.

A_{753} encoded a protein which shares identity with RelB family of TASs, described, amongst others, in *E. coli* [22]. The genes T_{133} and A_{132} were reported to encode an AAA-ATPase and a subtilisin-like serine protease, respectively. A functional TAS (ietAS) with compelling protein similarity exists in *Agrobacterium tumefaciens* [23]. A_{890} and T_{731} were also denominated as belonging to the Abi protein family, according to TASmania and A_{525} was assigned to belong to MraZ protein family, which is similar to the TAS MazEF of *E. coli* [24, 25]. Different types of TAS have been described based on their mode of action and the six TAS identified in our study represent type II and type IV TAS (**Table 1**).

Detection of transcripts and proteins encoded by candidate TAS

We tested the presence of transcripts covering the genes encoding the six candidate TAS. Therefore, reverse transcription PCR was performed on *Mmc* GM12 RNA with primers targeting the genes encoding candidate toxins, antitoxins and the whole putative two-gene operons. We isolated 24 - 35 µg total RNA from 20 mL cultures. A PCR with primers targeting 16S rRNA did not reveal any amplicons confirming absence of DNA in the RNA preparation. Transcripts of all 6 TAS investigated except for A_{890} were detected via reverse transcription PCR (**Figure S1**).

Afterwards we investigated the presence of candidate toxins and antitoxins using a shot gun proteomics approach, in which we harvested GM12 at one time point, specifically during the log growth phase. Mass spectrometry showed that in *Mmc* GM12 protein abundance of A_{524} is medium, whereas A_{132}, A_{753} and A_{161} as well as T_{133} and T_{731} are available in low abundance. We arbitrarily assigned relative abundance thresholds based on the quartile of the $\log_{10}$ (mean dNSAF) values distribution: value -3.8 of the lower quartile (Q1) defined as low/medium boundary and value -2.8 of the upper quartile (Q3) defined as medium/high boundary. For reference, house-keeping enzymes dihydrolipoamide S-acetyltransferase, adenylate kinase,

glucose-6-phosphate isomerase, DNA-directed RNA polymerase beta chain, guanylate kinase, DNA gyrase subunit B and recombination protein present $\log_{10}$ (mean dNSAF) values of -2.0, -2.5, -2.5, -2.6, -2.8, -3.0 and -4.4, respectively. The other candidate toxins and antitoxins were below the detection limit of the mass spectrometry analysis (**Figure 2, Table S2**). In summary only the candidate toxin and antitoxin of $TAS_{133/2}$ have been detected using the shot gun approach, for the TAS.

High conservation in the organization of the *Mmc* genomes

Each of the 15 genomes was assembled into one circularized chromosome and the chromosomes were rotated based on the gene *dnaA*. Key features of each genome are displayed in **Table S3**. The size of the 15 genomes ranged from 1,019,884 to 1,172,410 bp and a G+C content of 23.7 %. All genomes contained 908 (± 93) CDS, 30 tRNAs, two rRNA operons, and 1 tmRNA each. The functional annotation, based on BLASTP of the CDS against a UniProtKB snapshot, revealed an average of 392 hypothetical proteins (~45% of the total annotated CDS) for each genome. In terms of genome organization, we observed a high level of syntheny **(Figure S2)**. Only strains 152/93 and C260/4 had a large inversion of more than 100.000 bp, which was confirmed by PCRs. Strain 152/93 contained a plasmid with a size of 1.875 bp, which was highly similar to pKMK1 [26] and p*Mmc*-95010 [27] detected in strains GM12 and 95010, respectively.

Distribution of the six candidate TAS in other mycoplasmas

Next, we were interested to investigate the distribution of the six candidate TAS in different strains of *Mmc* and to extend this analysis to members of the so called '*M. mycoides* cluster', which comprises four additional closely-related ruminant pathogens besides *Mmc*. The presence of genes was investigated by TBLASTN employing complete genome sequences.

Different *Mmc* strains showed that the presence of candidate TAS was not clonal, meaning phylogenetically closely related strains had not necessarily the same set of candidate TAS. Specifically, $TAS_{752/3}$ was present in most strains, except C260/4 and Wi8079, which lacked A_{753}. $TAS_{133/2}$ and $TAS_{160/1}$ were only present in strains 7730, My-I, My-325, My-5 and My-18 (**Figure 3A, Table S4**). We revealed that our candidate TAS were also not present in all members of the '*M. mycoides* cluster' (**Figure 3B, Table S4**).

Functionality testing of candidate TAS using heterologous expression

Three of the six candidate TAS were chosen for further characterization. These ones included two candidate TAS identified via TASmania, namely $TAS_{160/1}$ and $TAS_{752/3}$, whereby $TAS_{160/1}$ represented the candidate system with the overall highest score (e-value of 1.2e-53 and 3.8e-49) and $TAS_{752/3}$ represented the candidate system with the lowest score among the five pairs (e-value of 3.5e-9) identified. Moreover, we included the candidate $TAS_{133/2}$ in our studies, since it was suspected to be a TAS because of polar effects of transposon insertions [15]. We aimed to test toxicity of candidate toxins using heterologous expression. Since mycoplasmas lack a cell wall and represent minimal organisms, we opted for testing heterologous expression in different recipients such as *E. coli*, *B. subtilis* and *M. capricolum*. Consequently we started with *E. coli*, which has been used to confirm TAS in both GRAM-negative and GRAM-positive bacteria [28]. In this bacterial species a bigger toolbox was available than for *Mycoplasma*, like expression vectors with inducible promotors and fast and efficient transformation protocols. Subsequently, genes encoding candidate toxins and antitoxins were cloned into *E. coli* using the established and robust pBAD/His expression system. Heterologous expression confirmed only a negative effect on bacterial growth for the toxin T_{133}, while the other two candidate toxins and all three antitoxins tested did not affect the growth of *E. coli* after induction. As expected, growth was only affected when expression of T_{133} was induced, but not when it was

repressed. Immunoblotting verified expression of recombinant proteins after induction for all cloned genes (**Figure S3A**). Specifically, four hours post induction, the OD_{600} of *E. coli* transformed with pBAD7His-T_{133} decreased drastically, compared to the various controls (**Figure 4A and Figure S3B**). Interestingly, we observed a phenotype characterized of clumping of *E. coli* cells later in the growth phase in induced *E. coli* cells harboring the vector with T_{133}. Then we visualized *E. coli* morphology of those cells using scanning electron microscopy. Visualization revealed that the cell shape started to alter four hours post induction, specifically a fraction of the induced cells was elongated, others were Z-shaped. After seven hours post induction, many cells seem to have burst with only the cell wall remaining visible and a large fraction of cells displayed blebbing at their poles as well as elongation (**Figure 4B**). Empty cell walls clumped together, leading to the clumping observed in liquid cultures by the naked eye. In contrast, cell morphology of all other constructs remained normal (**Figure S3C**). We tested the candidate TAS subsequently in another model organism, namely *B. subtilis.* The rationale behind testing heterologous expression in a GRAM-positive model bacterium was rooted in the closer phylogenetic distance of *B. subtilis* to mycoplasmas that are closely related to the GRAM-positive bacteria and specifically to Clostridia. For these heterologous expression experiments we used the commercial expression system based on pHT01 vector cloned into *B. subtilis* strain 168 Marburg. Construction of the different shuttle plasmids in *E. coli* resulted in six plasmids, each containing a gene encoding either a candidate toxin or antitoxin belonging to the three candidate TAS to be functionally tested. All plasmids except the one containing T_{133} revealed transformants in *B. subtilis*. Since all other plasmids were transformable, toxicity associated with T_{133} is likely to have resulted in absence of viable transformants. Even without IPTG-induction, the promotor of pHT01 causes a low background expression level, which might account for toxic effects of T_{133}. Out of the two toxins transformed successfully and tested subsequently in a growth assay, only the toxin T_{752} affected

bacterial growth after induction with IPTG, while the other toxin and antitoxins tested had growth curves comparable to *B. subtilis* carrying the empty vector pHT01. Specifically, two hours after IPTG induction, cell density of *B. subtilis* harboring T_{752} started to drop, compared to the other induced toxins and antitoxins, indicating lysis (**Figure 5A**, **Figure S4A**). Laser scanning micrographs of *B. subtilis* harboring T_{752}, showed an altered cell morphology compared to non-induced cells or cells harboring the empty vector (induced or non-induced) (**Figure 5B**), (**Figure S4B**). A large fraction of cells harboring T_{752} burst, shrunk or had holes on the cell surface. Many cells observed during binary fission had one half burst and the other half intact.

Finally, we took advantage of the availability of stably replicating plasmids available for selected members of the '*M. mycoides* cluster'. Since our genome comparisons showed that *Mcap* did not harbor any of the three candidate TAS to be investigated for functionality, *Mcap* represented a "natural knock-out" and was an ideal candidate for heterologous expression. We constructed a set of 4 plasmids for each TAS including the entire TAS under the control of the natural promotor, the antitoxin under the control of the natural promotor and the toxin under the control of the natural promotor as well as the strong spiralin promotor. The cloning of the different plasmids was done via Gibson assembly in *E. coli*. Sequence-verified recombinant plasmids (**Supplementary file S1**) were transformed into *Mcap* and transformation efficacies were monitored to assess toxicity. Transformation of only the antitoxins yielded same amount of transformants as transformation of the empty vector (between 10^5 and 10^6 transformants per µg plasmid). When only the toxins were transformed, 2 logs less transformants were observed compared to the empty vector, which was a significant result. Number of transformants harboring the toxin with the natural promotor compared to the ones containing the spiralin promotor did not differ significantly, except for T_{133} under the control of the spiralin promotor, which did not result in any transformants at all. Transformation rates of the entire

TAS did not differ to the empty vector or the individual antitoxins indicating neutralization of the toxic effects by the antitoxin (**Figure 6**).

Assessment of vector and insert presence was tested in 3-5 transformants per transformation experiment. It confirmed the presence of antitoxins and entire TAS as expected. *Mcap* cells transformed with the toxin T_{133} under the control of the natural promotor, were found to contain at most partial toxin sequences. We confirmed the presence of T_{752} sequence with its natural promotor in a fraction of the transformants investigated, but transformants of the toxin under the control with the spiralin promotor did not contain T_{752} sequences. The sequence of T_{160} were found in all the examined clones with natural and spiralin promotor.

Donor-recipient phylogenetic distance impacts functional confirmation of TAS

Toxicity testing has been carried out in the three recipient species *E. coli*, *B. subtilis* and *Mcap* listed from most to least phylogenetic distance to the TAS donor species *Mmc*. We started testing the two components of the TAS individually in *E. coli* using the established expression system based on pBAD/His. Only T_{133} conferred toxic activity to its recipient upon induction of expression, indicating $TAS_{133/2}$ to be functional. Next, we proceeded to test the systems in *B. subtilis*, which is phylogenetically much closer to *Mmc* than *E. coli*, but likewise consists of a much bigger proteome and a cell wall, factors that are likely to interfere with TAS functionality. The pHT01 vector used has some basal expression, since its promotor is not tight. It was not possible to transform the vector containing T_{133} into *B. subtilis*, indicating toxicity affecting transformation. Additionally, the growth of the clone carrying T_{752} was impacted after induction of expression. Therefore, two out of three TAS tested functional in *B. subtilis*. In *Mcap* all TAS tested functional and moreover the antitoxins neutralized the toxins. In summary, heterologous expression systems confirmed functionality influenced by donor-recipient phylogenetic distance.

Discussion

This study aimed to identify and to produce proof of the functionality of toxin antitoxin systems (TAS) in minimalistic mycoplasmas for the first time. Therefore, we employed our model organism, the highly pathogenic *Mycoplasma mycoides* subsp. *capri* strain GM12. Many pathogenic mycoplasmas are associated with chronic infections, which theoretically suggests a role for TAS to support existence in a stealth mode that protects the mycoplasmas from immune responses. In fact, live *Mycoplasma mycoides* subsp. *mycoides*, the causative agent of contagious bovine pleuropneumonia, have been isolated from lung sequestra >6 months after experimental infection [10] and the same mycoplasmas survived even in the presence of high antibody titers against the latter. The *in silico* analysis of strain GM12 revealed 18 chromosomally encoded putative candidate TAS elements of which five candidate TAS with the lowest TASmania output e-values were short-listed for our study. In *Mycobacterium tuberculosis*, a deathly human respiratory pathogen with a much larger genome, at least 79 TAS have been reported to be involved in numerous mechanisms regarding cellular processes such as cell death, persistence and virulence [29-31]. In contrast, *Campylobacter jejuni*, a human pathogen causing diarrhea, has been reported to contain no more than three TAS, which underlines a great variety in the abundance of TAS in different prokaryotic genera [29]. So far, functional TAS in mycoplasmas have never been convincingly shown but only indicated *in silico* based on sequence similarity to other TAS [32]. In this study, we focused on the characterization of the TAS with the lowest e-values, since they provided the biggest odds of having a functional TAS. We added the candidate $TAS_{133/2}$, which was proposed recently [15] based on the analysis of a transposon insertion library of JCVI-syn2.0, a synthetic cell controlled by a drastically reduced genome [2]. These six candidate TAS were grouped into types II and IV (**Table 1**) systems. In type II systems the proteinaceous antitoxin is binding to the toxin to prevent its action, in type IV systems the antitoxin competitively binds the toxin

cell target. First, we aimed to identify transcripts and protein signatures of the six systems during in vitro growth indicating a biological function of the genes investigated. We identified transcripts of all TAS elements except for A_{890} supporting a role of transcribed genes in the physiology of GM12. The absence of a transcript for A_{890} does not exclude its transcription, since low levels of transcription and a high turnaround time of transcripts can cause transcripts to be below the detection limit. Protein signatures encoded by the six TAS elements were detected for the entire $TAS_{133/2}$ and the individual elements of four TAS, namely A_{161}, A_{524}, T_{731} and A_{753}. The only system we had no proteomic signatures was the $TAS_{889/0}$ for which we did not detect a transcript of A_{890}. The detection of proteomic signatures in five out of six candidate TAS using a generic proteomics approach indicates a high probability of functionality especially for the $TAS_{133/2}$. The complete genomes of 16 *Mmc* strains revealed a high level of synteny, only two strains had a large inversion in contrast to the other strains. Interestingly, three out of six TAS were present in all 16 *Mmc* genomes investigated, while phylogenetic clades sometimes also had different TAS fingerprints (**Figure 3A**) making horizontal gene transfer likely to have acted on TAS acquisition or loss. Investigation of genomes of the five members of the *M. mycoides* cluster, which consists of three species (two species contain two subspecies) [33], also confirmed the presence of $TAS_{752/3}$, $TAS_{731/0}$ and $TAS_{525/4}$ in all species investigated (**Figure 3B**) pointing towards old rather conserved acquisitions and a certain plasticity of the genome with respect to TAS. The '*M. mycoides* cluster' is evolutionary young, since its common ancestor dates back 10,000 years [33] coinciding with the start of ruminants' domestication. Therefore, these different TAS fingerprints likely formed within the last 10,000 years and horizontal gene transfer [34-36] is likely to have contributed to it.

Next, we tested functionality and shortlisted three candidate TAS for this purpose, based on at least one of the following arbitrary criteria i) a low e-value (<10e-7), ii) TAS-related name for

the nearest Pfam annotation of the TASmania HMM profile that hit the locus, iii) TAS-related gene description and iv) presence of candidate toxin and cognate antitoxin in our proteomic analysis. We selected $TAS_{133/2}$, since protein signatures were reported for its toxin and cognate antitoxin, $TAS_{160/1}$, since it was the type IV system with the highest TASmania score and $TAS_{752/3}$, and since it was suggested to be a type II system and its toxin and cognate antitoxin encoding gene had gene annotations. For functional testing we established a model organism-based approach by expressing recombinant toxins and antitoxins in the different recipients *E. coli* and *B. subtilis* employing expression plasmids with inducible promotors as well as transforming the candidates in the closely related *Mycoplasma capricolum* subsp. *capricolum*. We started to test toxicity of candidate toxins in *E. coli*, which has been done for other candidate TAS of GRAM-positive bacteria, e.g. Streptomyces [37] or Mycobacteria [28]. Unexpectedly, although being high score candidates, two out of three candidate TAS did not test positive in *E. coli*. Only recombinant T_{133}, annotated as subtilisin-like serine protease, had a toxic effect on the growth of *E. coli* LMG194. Serine proteases cleave peptides or proteins. A role of serine proteases as toxins in TAS has not been reported except for IetS [23] in the GRAM-negative plant pathogen *Agrobacterium tumefaciens*, a toxin which was shown to be involved in plasmid stability. Heterologous expression of T_{133} in *E. coli* resulted in cell clumping in liquid culture and elongated and filamented cells. The observed morphological changes can be attributed to either direct toxic effects or a stress response of *E. coli* towards the recombinant T_{133}, which should be investigated in future studies. Cell filamentation has been reported to occur as an SOS response upon DNA damage in other bacteria [38, 39]. Heterologous expression in *B. subtilis* revealed toxicity of recombinant T_{133} (plasmid carrying T_{133} was not transformable) and of T_{752}, which had a toxic effect on the growth. The latter encodes for a fic protein, which are known in bacteria to disrupt the DNA topology via adenylation and causes growth arrest [40]. Finally, functionality of all three TAS investigated

344 was shown in the transformation experiments carried out with *Mcap*. These experiments clearly
345 also showed the capacity of the antitoxins to neutralize the effects of the toxins. Interestingly,
346 the type IV system $TAS_{160/1}$ only showed functionality in *Mcap*, probably due to the fact that
347 in such systems toxin and antitoxin bind to the same target, which was probably only available
348 in a mycoplasma.
349 In conclusion, this study identified six candidate TAS and tested functionality of three out of
350 the six chromosomally encoded TAS in *Mmc* GM12. Functionality of the three candidate TAS
351 was shown, as expression of only the toxin results in perturbations of cell vitality or in cell
352 death whereas the cognate antitoxin compensated the toxin-induced effects completely.
353 Further, we evaluated different model organisms as *E. coli*, *B. subtilis* and *Mycoplasma*
354 *capricolum* for heterologous expression of TAS. According to our results, toxin action seems
355 to be dependent on phylogenetic proximity towards the bacterial species from which candidate
356 TAS originate. TAS patterns were different in different *Mycoplasma* species and subspecies
357 indicating a level of plasticity of the mycoplasmas' genomes with respect to TAS. Since
358 mycoplasmas are minimal organisms [11] amendable to synthetic genomics techniques [41],
359 their host-pathogen interactions can be investigated in the native host [17, 18, 42] and as they
360 contain only a limited number of TAS, they represent an ideal model organism to study the
361 role of TAS in pathogenicity.

362 ## Materials and methods

363 ### *In silico* identification of candidate TAS

364 Identification of candidate TAS in *Mmc* strain GM12 [16] was performed by employing the
365 TASmania discovery pipeline [20], which uses data mining on the Ensembl Bacteria database
366 [43] to identify candidate toxin and antitoxin proteins. The e-value was set to the default value
367 of 1e-05. TAS candidates to be characterized in the study had the following minimal
368 requirements: an e-value lower than 1e-07, a protein family (pfam) describing known TAS and
369 gene description indicating possible candidates. If TAS candidates were without a counterpart
370 (toxin or antitoxin), the counterparts were manually selected using 'guilt by association',
371 considering the cognate loci of the respective gene as the partner of a two gene operon.
372 Intergenic regions close to toxin and antitoxin genes on the *Mmc* GM12 genome were analyzed
373 using BPROM (Softberry) [44] to identify putative promotor regions.

374

375 ### Bacterial strains and plasmids used for cloning in this study

376 Plasmid based on pBAD/His (Invitrogen) or pHT01 (MoBiTech) and pMYCO1 were
377 constructed in *E. coli* DH5α (Takara) and Stellar™ (Takara), respectively. Heterologous
378 expression based on pBAD/His and pHT01 was done in *E. coli* LMG194 (Invitrogen) and *B.*
379 *subtilis* 168 Marburg (MoBiTech), respectively. The restriction-free *M. capricolum* subsp.
380 *capricolum* mutant strain *M. capricolum* RE(–) [41] was used as recipient for transformation
381 experiments involving pMYCO1-derived plasmids [45].

382

383 ### Detection of transcripts for candidate TAS

384 *Mycoplasma mycoides* subsp. *capri* (*Mmc*) strain GM12 was grown in 10 ml SP5 medium at
385 37˚C until the culture reached pH 6.5. Subsequently, the culture was centrifuged at 4,255 x *g*
386 at 10˚C for 15 min. The supernatant was discarded and the bacterial cell pellet was used for

RNA isolation. RNA was isolated using the Zymo Research Quick-RNA Fungal/Bacterial Miniprep™ kit. Briefly, 800 µl of RNA Lysis Buffer were added to the pellet and the protocol was followed starting at step 4 of the manual. After isolation, a DNase treatment was performed using the Clean & Concentrator™ -5 kit (ZymoResearch), omitting the first step of the protocol (addition of Binding Buffer) and using the IICR columns provided in the kit. Reverse transcription PCR was performed using SuperScript™ IV RT Mix (Invitrogen) and 2x Platinum™ SuperFi™ RT-PCR Master Mix (Invitrogen) using primers No. 59-82 listed in **Table S4**. In brief, 12.5 µl of 2x Platinum™ SuperFi™ RT-PCR Master Mix, 0.25 µl SuperScript™ IV RT Mix, 1.25 µl per primer (10 µM), 1µl DNase treated RNA (~ 32 ng) and water up to a volume of 25 µl were mixed per sample. Amplicons were visualized on a 1% agarose gel.

Proteomic analysis

Strain GM12 was grown in 50 mL of SP5 media until mid to late logarithmic phase (pH of media at harvest was 6.5) and centrifuged at 3,000 x *g* for 20 min. Cells were washed three times with PBS and pellets were kept at -80 for subsequent analysis. The protein concentration was measured using the Pierce BCA Protein Assay Kit (ThermoScientific) according to vendor's instructions. Samples for mass spectrometry analysis were prepared following standard protocols [46]. Briefly, cell pellets were thawed on ice and lysed in 8M urea/100mM Tris-HCl; proteins were precipitated in cold acetone over-night and denatured with 8M urea/50mM Tris-HCl, then digested with trypsine over-night at room-temperature in 1.6M urea /20mM Tris-Hcl /2mM $CaCl_2$. Enzymatic digestion was stopped by adding 1/20-volume of 20% (v/v) tri-fluoroacetic (TFA). The digests were analyzed by liquid chromatography (LC)-MS/MS (PROXEON coupled to a QExactive HF mass spectrometer, ThermoFisher Scientific). Samples were further processed against custom databases by Transproteomics pipeline (TPP)

412 tools [47]. Four database search engines were used: Comet [48], Xtandem [49], MSGF [50]
413 and MyriMatch [51]. Each search was followed by the application of the PeptideProphet tool
414 [52]; the iProphet [53] tool was then used to combine the search results, which were filtered at
415 the false discovery rate of 0.01; furthermore, the identification was only accepted if at least two
416 of the search engines agreed on the identification. The decoy approach was used for such
417 custom databases containing standard entries. Protein inference was performed with
418 ProteinProphet. For those protein groups accepted by a false discovery rate filter of 0.01, a
419 Normalized Spectral Abundance Factor (NSAF) [54] was calculated based on the peptide to
420 spectrum match count; shared peptides were accounted for by the method published elsewhere
421 [55].
422
423 **Cloning of genes encoding candidate toxins and antitoxins in *Escherichia coli***
424 *E. coli*-codon optimized synthetic genes encoding candidate toxins or antitoxins were
425 synthesized and cloned into pUC57 and sequence-verified by GenScript (**Supplementary File**
426 **S1)**. For ligation into the expression vector pBAD/His, genes to be cloned, were PCR-amplified
427 using primers that contained restriction sites for *EcoRI* and *SacI* (**Table S5**, primers No. 1-6)
428 and the high-fidelity polymerase Q5 (New England Biolabs) according to vendor's manual.
429 Amplicons were purified using the High Pure PCR Product Purification Kit (Roche) and
430 afterwards restricted with *EcoRI* (New England Biolabs) and *SacI* (New England Biolabs)
431 followed by another purification using the above-mentioned kit. Toxin genes to be cloned were
432 retrieved from the plasmids that contained the synthetic genes via restriction followed by gel
433 purification. Restricted fragments to be cloned were ligated into the *EcoRI* and *SacI* restricted
434 pBAD/His using T4 Ligase (Promega) before being heat shock-transformed into chemically
435 competent *E. coli* DH5α (Takara) or Stellar™ (Takara) using standard protocols [56].
436 Recombinant plasmids from transformants were isolated using the QIAprep® Spin Miniprep

Kit (Qiagen) and sequence-verified via Sanger sequencing (Microsynth) with specific primers (**Table S5**, primers No. 7-8). Sequence-verified plasmids were heat shock-transformed into chemically competent *E. coli* LMG194 for subsequent expression. Transformants were verified as described above and stored at -80 ˚C for subsequent experiments.

Functional testing of candidate *Mycoplasma* TAS using heterologous expression in *E. coli*

Growth curves of *E. coli* LMG194 containing inducible expression vector pBAD/His carrying genes encoding individual candidate toxins and antitoxins were performed in 96-well plates (Tissue culture test plates, 92096, TPP) and monitored over a period of seven hours. All clones were cultured in LB medium supplemented with 50 µg/mL ampicillin. Twenty µL of overnight cultures of clones to be tested were mixed with 180 µL LB supplemented with either 0.2% (w/v) arabinose or 0.2% (w/v) glucose to induce or repress protein expression, respectively. Cultures in 96-well plates were incubated at 37 ˚C under agitation (500 rpm) using a ThermoMixerC (Eppendorf). Optical density was measured at 600nm using the VERSAmax plate reader (Bucher Biotec, Basel, Switzerland). Final datasets were obtained from three biological replicates (each biological replicate consisted of three technical replicates). To assess the significance of the heterologous expression on growth of the clones at every time point, we applied a three-way (time, treatment, construct) repeated-measures ANOVA and decomposed into post hoc tests based on pairwise comparisons with a Bonferroni adjustment of the p-value. The statistical analysis was done using R version 3.6.2.

Detection of recombinant proteins using immunoblots

Heterologous expression in *E. coli* was verified by immunoblot using anti-HIS antibodies tagging the recombinant fusion proteins. Briefly, 200 µL of overnight culture were mixed with 20 ml of LB supplemented with 50 µg/mL ampicillin and arabinose (final concentration 0.2%).

462 Cultures were grown on a shaking incubator at 220 rpm (Lab-Shaker) at 37 ˚C and samples of
463 1 mL were sequentially removed at several time points for subsequent analysis. As controls
464 served the same clones grown in the same media except that arabinose was exchanged with
465 glucose (final concentration 0.2%). Samples were spun down at 16,100 x *g* at room temperature
466 for 3 min. The supernatants were discarded, the pellets were resuspended in PBS (Merck) and
467 the protein concentration was determined using the Pierce™ BCA Protein Assay Kit
468 (ThermoScientific). Immunoblotting was basically carried out as described recently [18].
469 Briefly, 0.1 mg of proteins in the cell pellet were separated onto a 12% SDS-PAGE gel using
470 standard procedures [56]. Size separated proteins were transferred onto a 0.2 µm pore-size
471 nitrocellulose membrane (BIO RAD) using the Trans-Blot® Turbo Transfer System (BIO
472 RAD) at 25 volts, 1.0 A for 30 min. PBS supplemented with 0.1% Tween-20 (Merck) and 2%
473 BSA (Sigma) served as blocking buffer and monoclonal mouse-derived anti-HIS antibody
474 (LS-C57341, LsBio) and HRP conjugated goat anti-mouse IgG antibody (AP308P, Sigma)
475 served as primary and secondary antibodies, respectively. Primary antibodies were diluted in
476 blocking buffer at 1:1,000 and incubated with the membrane for 1 hour, afterwards the
477 membrane was washed 3 times in PBS supplemented with 0.1% Tween-20 for 10 min. Then
478 the membrane was incubated with the secondary antibody diluted at 1:70,000 in blocking
479 buffer for 1 hour. After three washes as done before the membrane was incubated with
480 SuperSignal™ West Pico PLUS Chemiluminescent Substrate (ThermoScientific) according to
481 manufacturer's recommendations. Chemiluminescence was visualized with the CCD-camera
482 Fusion FX (Vilber) and analyzed by the software Evolution.
483
484 **Cloning of genes encoding candidate toxins and antitoxins in *Bacillus subtilis***
485 Synthetic genes to be cloned into *B. subtilis* were first cloned into *E. coli* using the shuttle
486 vector pHT01 (MoBiTec). Therefore, genes were PCR-amplified using synthetic genes cloned

into pUC57 (see above) as template, primers that contained restriction sites for *BamHI* and *XmaI* or *XbaI* (**Table S5**, primers No. 9-16 and 95-98) and the high-fidelity polymerase Q5 (New England Biolabs) according to vendor's manual. Amplicons were purified using the High Pure PCR Product Purification Kit (Roche) and afterwards restricted with *BamHI* (ThermoScientific) and *XmaI* (ThermoScientific) or *XbaI* (ThermoScientific) followed by another purification step using the above-mentioned kit. The restricted amplicons were ligated into the *BamHI* and *XmaI* (*BamHI* and *XbaI*) restricted pHT01 using T4 Ligase (Promega) before being heat shock-transformed into chemically competent *E. coli* Stellar™ (Takara) following standard protocols [56]. *E. coli* Stellar™ was grown on LB media supplemented with ampicillin at 50 µl/mL. Colony PCR was performed with primers No. 17-24 and 99-102 (**Table S5**). Recombinant plasmids from transformants were isolated using the QIAprep® Spin Miniprep Kit (Qiagen) and sequence verified via Sanger sequencing (Microsynth) with specific primers (**Table S5**, No. 25-26). Sequence-verified plasmids were transformed into *Bacillus subtilis* 168 Marburg (MoBiTec) using vendor's protocols. Therefore, we followed the protocol for making naturally competent cells. Transformants were selected on agar plates containing 5 µg/mL chloramphenicol. Transformants were lysed as described elsewhere [57] and presence of plasmids was confirmed via PCR targeting cloned genes. Clones were stored at -80 ˚C for subsequent experiments.

Functional testing of candidate TAS using heterologous expression in *B. subtilis*

Growth curves of *B. subtilis* 168 Marburg containing inducible expression vector pHT01 carrying genes encoding individual candidate toxins and antitoxins were performed in 96-well plates (Tissue culture test plates, 92096, TPP) and monitored over a period of seven hours. All clones were cultured in LB medium supplemented with 5 µg/mL chloramphenicol (Serva). Overnight cultures of *B. subtilis* 168 Marburg were diluted to an OD_{600nm} of 0.15 in a total

512 volume of 5 mL, which was subsequently incubated at 37 ˚C. When cultures reached an OD_{600}
513 of 0.7-0.8, IPTG (Roche Diagnostics) was added to a final concentration of 1 mM for induction
514 of heterologous protein expression. Cultures in 96-well plates were incubated at 37 ˚C under
515 agitation (500 rpm) using a ThermoMixerC (Eppendorf). Optical density was measured at 600
516 nm using the VERSAmax plate reader (Bucher Biotec). Final datasets were obtained from three
517 biological replicates (each biological replicate consisted of three technical replicates).
518 To assess the significance of the heterologous expression on growth of the clones at every time
519 point, we applied a three-way (time, treatment, construct) repeated-measures ANOVA and
520 decomposed into post hoc tests based on pairwise comparisons with a Bonferroni adjustment
521 of the *p*-value. The statistical analysis was done using R version 3.6.2.
522
523 **Cloning of genes encoding candidate toxins and antitoxins into *Mycoplasma capricolum***
524 **subsp. *capricolum***
525 The three candidate TAS operons, as well as each of the genes encoding candidate toxins and
526 antitoxins, were individually cloned into pMYCO1. Candidate genes or operons were PCR
527 amplified using Q5 high fidelity DNA polymerase (New England Biolabs) according to
528 manufacturer's instructions using primers (No. 27-49) listed in **Table S5**. DNA assembly was
529 performed in *E. coli* using the NEBuilder HiFi DNA Assembly kit (New England Biolabs)
530 following manufacturers' instructions. When necessary, the natural promoters of each of the
531 TAS were amplified independently and positioned in frame with their respective candidate
532 toxins. Similarly, the spiralin promoter was amplified from the plasmid pMT85tetM-PSlacZ-
533 pRS313 (GenBank accession number KX011460) and assembled upstream of each toxin. All
534 the constructions were sequenced using primers No. 57 and 94 (**Table S5**).
535

536 **Functional testing of candidate TAS using heterologous expression in *M. capricolum***
537 **subsp. *capricolum* (RE-)**

538 *M. capricolum* subsp. *capricolum* (*Mcap*) (RE-) was selected to probe functionality of the three
539 candidate TAS as none of the latter appeared to be present in its genome (**Figure 3B**). All 12
540 pMYCO1-based constructs were transformed into *Mcap* (RE-) as previously described [58]
541 using 1 µg of plasmid DNA. Three biological replicates including three technical replicates per
542 biological replicate were carried out. Transformants were passaged for three consecutive
543 rounds in 1ml SP5 medium supplemented with 5 µg/mL tetracycline and incubated at 37 ˚C to
544 confirm the resistant phenotype. Transformants were screened using primer pairs specific for
545 the inserted TAS elements (**Table S5**, No. 50-58). Numbers of transformants were used to
546 analyse transformation efficacies. An ordinary one-way ANOVA test with Tukey's multiple
547 comparison test was applied (GraphPad Prism version 8.0.0, San Diego, California USA).
548

549 **Scanning electron microscopy (SEM) of *E. coli* and *B. subtilis* recombinant clones**

550 The morphology of *E. coli* and *B. subtilis* cells upon toxin induction was investigated by
551 scanning electron microscopy. Clones to be visualized were cultured and expression of the
552 candidate toxins was induced as described above. Samples collected during expression (1 ml)
553 were centrifuged at 1,500 x *g* at room temperature for 3 min. The pellets were washed 3 times
554 with 1 ml PBS and finally resuspended in 250 µl PBS. Subsequently, 250 µl of 5%
555 glutaraldehyde (Merck) in 0.2M cacodylate buffer, pH 7.4, was slowly added to the samples
556 with gentle agitation. The tubes were stored at 4 ˚C until further processing. Fixed cells were
557 cytospun onto platinum-sputtered and PLL-coated coverslips (40 µl at 125 x *g*, 5 min). The
558 coverslips were then washed 3 times with 0.1M cacodylate buffer, pH 7.4, postfixed in 1%
559 OsO4 (Polysciences) in 0.1M cacodylate buffer for 30 min, washed 3 times again and
560 dehydrated in an ascending series of ethanol (70%, 80%, 94%, 100%, 100%, 100% ethanol at

561 room temperature for 15 min each). Samples were dried by evaporation of
562 Hexamethyldisilazane (Merck). Samples were coated with 15 nm of platinum in a high vacuum
563 coating unit (CCU-010; Safematic) and examined with a scanning electron microscope DSM
564 982 Gemini (Zeiss) at an accelerating voltage of 5 kV at a working distance of 4 mm.
565

566 **Isolation of genomic DNA from for next generation sequencing**

567 Mycoplasmas grown in 8 ml of SP5 medium overnight were pelleted at 4,255 x *g* at 10 ˚C for
568 15 min. The supernatant was discarded and gDNA was extracted using the Wizard Genomic
569 DNA purification kit (Promega) according to vendor's protocol. Plasmid DNA was extracted
570 from 10 ml overnight culture using QIAprep® Spin Miniprep Kit (QIAGEN) with the
571 following adaptations: additional washing with buffer PB and using the double of the
572 recommended volume of buffers P1, P2 and P3. DNA concentration and purity were
573 determined by agarose gel separation, Nanodrop (ND-1000 Spectrophotometer, Witec AG) and
574 Qubit Fluorometric quantification (Invitrogen).
575

576 **Next generation sequencing of *Mycoplasma mycoides* subsp. *capri* strains**

577 Sequencing was carried out at the Lausanne Genomic Technologies Facility using the PacBio.
578 Briefly, DNA was sheared in a Covaris g-TUBE (Covaris, Woburn, MA, USA) to obtain 10
579 kbp fragments. After shearing, the DNA size distribution was checked on a Fragment Analyzer
580 (Advanced Analytical Technologies, Ames, IA, USA). A barcoded SMRTbell library was
581 prepared using 480 ng of gDNA using the PacBio SMRTbell Template Express Prep Kit 2.0
582 (Pacific Biosciences, Menlo Park, CA, USA) according to the manufacturer's
583 recommendations. Libraries were pooled and sequenced with v3.0/v3.0 chemistry on a PacBio
584 Sequel instrument (Pacific Biosciences, Menlo Park, CA, USA) at 10 hours movie time, pre-
585 extension time of 2 hours, using one SMRT cell v3.

586

587 **Genome assembly, annotation and alignments**

588 Genomes were assembled from PacBio reads using the software Flye, version 2.6 [59].
589 Circularized genomes were polished with three rounds with the software Arrow [single-
590 molecule real-time (SMRT) Link version 8 package]. Plasmids were Sanger sequenced after
591 cloning into *E. coli* using pUC19. Genomes were rotated to the first nucleotide of the start
592 codon of the *dnaA* gene. Sequences were then annotated using Prokka, version 1.13 [60]. The
593 program Mauve (version 20150226) [61] was used for the construction of the genome
594 alignment of multiple *Mycoplasma* strains.

595

596 **Generation of a phylogenetic tree of members of the '*M. mycoides* cluster'**

597 The phylogenetic tree was generated using 16S rRNA sequences retrieved from GenBank. The
598 following strains were included in the analysis: *Mycoplasma mycoides* subsp. *capri* strain
599 GM12 (GenBank accession number NZ_CP001668.1), *Mycoplasma mycoides* subsp. *mycoides*
600 strain PG1^T (GenBank accession number BX293980.2), *Mycoplasma capricolum* subsp.
601 *capricolum* strain California kid^T (GenBank accession number NC_007633.1), *Mycoplasma*
602 *capricolum* subsp. *capripneumoniae* strain F38^T (GenBank accession number LN515398.1),
603 *Mycoplasma leachii* strain PG50^T (GenBank accession number NC_014751.1) and
604 *Mycoplasma putrefaciens* strain KS1^T (GenBank accession number NC_015946.1). The
605 software MEGA, version 10.0.5 [62] was used for construction of phylogenetic trees. For the
606 phylogenetic tree displaying the *M. mycoides* cluster, evolutionary history was inferred using
607 the Neighbor-Joining method and evolutionary distance was computed with Kimura 2-
608 parameter method. For statistical support of the phylogeny, 100 replicates were used for the
609 bootstrap test.

610

611 **Generation of phylogenetic trees of *Mmc* strains using whole genome sequences**

612 For tree generation, whole genome sequences of *Mycoplasma mycoides* subsp. *capri* strains
613 were used and *Mycoplasma mycoides* subsp. *mycoides* PG1^T was included as an outgroup.
614 Mapping of genomes was performed by the Reference sequence Alignment based Phylogeny
615 builder (REALPHY) [63]. For tree construction, the software MEGA (version 10.0.5) [62] was
616 used. Evolutionary history was inferred using the Neighbor-joining method. Evolutionary
617 distances were computed with Maximum Composite Likelihood method. Rate variation among
618 sites was modelled with a gamma distribution.

619

620 **Graphic representation of toxin and antitoxin presence on genomes of mycoplasmas**

621 A graphic representation of gene presence was generated based on TBLASTN similarity of
622 candidate toxin and antitoxin amino acid sequences and genomes of different mycoplasmas.
623 The presence and conservation of each toxin and antitoxin candidate was assessed using
624 TBLASTN [64] with *Mmc* GM12 amino acid sequences of candidate toxins and antitoxins as
625 query against whole genome sequences of different *Mycoplasmas* and *Mmc* strains. All
626 sequences with query coverage >99% and percent identity >80% were considered as being
627 present on the respective genome. If Query coverage was <55%, we did assume the candidate
628 toxin/antitoxin does not exist in the respective genome. In case the query coverage was >70%
629 but percent identity was <61%, a BLASTN was additionally performed to check for nucleotide
630 sequence similarity. If the nucleotide sequence identity query coverage of BLASTN was >80%
631 and percent identity >70%, we assumed the candidate toxin/antitoxin to be present on the
632 respective genome.

633

634 **Author contributions:** JJ designed the research. VH, FL, RSB, HAE, MHS performed the
635 research. VH, FL, HAE, LF, ManH and JJ analyzed the data. MarH provided *Mycoplasma*

636 *mycoides* subsp. *capri* strains, ManH the proteomics infrastructure. VH, FL and JJ drafted the
637 manuscript. All authors read and approved the final manuscript.
638

639 **Acknowledgements**

640 We thank Helga Mogel, Sybille Schwendener, Simon Feyer and Isabelle Brodard (University
641 of Bern, Switzerland) for their technical help. We thank Joerg Stülke for provision of the
642 *Bacillus subtilis* strain 168 Marburg and the plasmid pHT01. We thank Patrick Viollier, Sanjay
643 Vashee and Volker Thiel for valuable discussions.

644 **References**

645

646 1. Gibson DG, Glass JI, Lartigue C, Noskov VN, Chuang RY, Algire MA, et al.
647 Creation of a Bacterial Cell Controlled by a Chemically Synthesized Genome. Science.
648 2010;329(52):52-6. Epub 2010/05/22. doi: science.1190719 [pii]
649 10.1126/science.1190719. PubMed PMID: 20488990.

650 2. Hutchison CA, 3rd, Chuang RY, Noskov VN, Assad-Garcia N, Deerinck TJ, Ellisman
651 MH, et al. Design and synthesis of a minimal bacterial genome. Science.
652 2016;351(6280):aad6253. doi: 10.1126/science.aad6253. PubMed PMID: 27013737.

653 3. Rogers MJ, Simmons J, Walker RT, Weisburg WG, Woese CR, Tanner RS, et al.
654 Construction of the mycoplasma evolutionary tree from 5S rRNA sequence data. Proc Natl
655 Acad Sci U S A. 1985;82(4):1160-4. Epub 1985/02/01. doi: 10.1073/pnas.82.4.1160.
656 PubMed PMID: 2579388; PubMed Central PMCID: PMCPMC397214.

657 4. McGowin CL, Totten PA. The Unique Microbiology and Molecular Pathogenesis of
658 *Mycoplasma genitalium*. J Infect Dis. 2017;216(suppl_2):S382-S8. Epub 2017/08/26. doi:
659 10.1093/infdis/jix172. PubMed PMID: 28838077; PubMed Central PMCID:
660 PMCPMC5853509.

661 5. Waites KB, Xiao L, Liu Y, Balish MF, Atkinson TP. *Mycoplasma pneumoniae* from
662 the Respiratory Tract and Beyond. Clin Microbiol Rev. 2017;30(3):747-809. Epub
663 2017/05/26. doi: 10.1128/CMR.00114-16. PubMed PMID: 28539503; PubMed Central
664 PMCID: PMCPMC5475226.

665 6. Di Teodoro G, Marruchella G, Di Provvido A, D'Angelo AR, Orsini G, Di Giuseppe
666 P, et al. Contagious Bovine Pleuropneumonia: A Comprehensive Overview. Vet Pathol.

667 2020:300985820921818. Epub 2020/05/12. doi: 10.1177/0300985820921818. PubMed
668 PMID: 32390522.

669 7. Yatoo IM, Raffiq Parray O, Tauseef Bashir S, Ahmed Bhat R, Gopalakrishnan A,
670 Karthik K, et al. Contagious caprine pleuropneumonia - a comprehensive review. Vet Q.
671 2019;39(1):1-25. Epub 2019/04/02. doi: 10.1080/01652176.2019.1580826. PubMed PMID:
672 30929577.

673 8. Maes D, Sibila M, Kuhnert P, Segales J, Haesebrouck F, Pieters M. Update on
674 *Mycoplasma hyopneumoniae* infections in pigs: Knowledge gaps for improved disease
675 control. Transbound Emerg Dis. 2018;65 Suppl 1:110-24. Epub 2017/08/24. doi:
676 10.1111/tbed.12677. PubMed PMID: 28834294.

677 9. Liljander A, Sacchini F, Stoffel MH, Schieck E, Stokar-Regenscheit N, Labroussaa F,
678 et al. Reproduction of contagious caprine pleuropneumonia reveals the ability of convalescent
679 sera to reduce hydrogen peroxide production in vitro. Vet Res. 2019;50(1):10. Epub
680 2019/02/10. doi: 10.1186/s13567-019-0628-0. PubMed PMID: 30736863; PubMed Central
681 PMCID: PMCPMC6368817.

682 10. Schieck E, Liljander A, Hamsten C, Gicheru N, Scacchia M, Sacchini F, et al. High
683 antibody titres against predicted *Mycoplasma* surface proteins do not prevent sequestration in
684 infected lung tissue in the course of experimental contagious bovine pleuropneumonia.
685 Veterinary Microbiology. 2014;172(1-2):285-93. Epub 2014/06/02. doi:
686 10.1016/j.vetmic.2014.04.018. PubMed PMID: 24880898.

687 11. Citti C, Blanchard A. Mycoplasmas and their host: emerging and re-emerging
688 minimal pathogens. Trends Microbiol. 2013;21(4):196-203. Epub 2013/02/20. doi:
689 10.1016/j.tim.2013.01.003. PubMed PMID: 23419218.

690 12. Lobato-Marquez D, Diaz-Orejas R, Garcia-Del Portillo F. Toxin-antitoxins and
691 bacterial virulence. FEMS Microbiol Rev. 2016;40(5):592-609. Epub 2016/08/01. doi:
692 10.1093/femsre/fuw022. PubMed PMID: 27476076.

693 13. Song S, Wood TK. Toxin/Antitoxin System Paradigms: Toxins Bound to Antitoxins
694 Are Not Likely Activated by Preferential Antitoxin Degradation. Adv Biosyst.
695 2020;4(3):e1900290. Epub 2020/04/16. doi: 10.1002/adbi.201900290. PubMed PMID:
696 32293143.

697 14. Kannan TR, Baseman JB. ADP-ribosylating and vacuolating cytotoxin of
698 *Mycoplasma pneumoniae* represents unique virulence determinant among bacterial
699 pathogens. Proc Natl Acad Sci U S A. 2006;103(17):6724-9. Epub 2006/04/18. doi:
700 0510644103 [pii]

701 10.1073/pnas.0510644103. PubMed PMID: 16617115; PubMed Central PMCID:
702 PMC1458948.

703 15. Hutchison CA, 3rd, Merryman C, Sun L, Assad-Garcia N, Richter RA, Smith HO, et
704 al. Polar Effects of Transposon Insertion into a Minimal Bacterial Genome. J Bacteriol.
705 2019;201(19). Epub 2019/07/03. doi: 10.1128/JB.00185-19. PubMed PMID: 31262838;
706 PubMed Central PMCID: PMCPMC6755753.

707 16. DaMassa AJ, Brooks DL, Adler HE. Caprine mycoplasmosis: widespread infection in
708 goats with *Mycoplasma mycoides* subsp *mycoides* (large-colony type). Am J Vet Res.
709 1983;44(2):322-5. Epub 1983/02/01. PubMed PMID: 6338774.

710 17. Jores J, Schieck E, Liljander A, Sacchini F, Posthaus H, Lartigue C, et al. In vivo role
711 of capsular polysaccharide in *Mycoplasma mycoides*. The Journal of Infectious Diseases.

712 2019;219(10):1559-63. Epub 2018/12/13. doi: 10.1093/infdis/jiy713. PubMed PMID:
713 30541131.

714 18. Jores J, Ma L, Ssajjakambwe P, Schieck E, Liljander A, Chandran S, et al. Removal
715 of a Subset of Non-essential Genes Fully Attenuates a Highly Virulent *Mycoplasma* Strain.
716 Front Microbiol. 2019;10:664. Epub 2019/04/20. doi: 10.3389/fmicb.2019.00664. PubMed
717 PMID: 31001234; PubMed Central PMCID: PMCPMC6456743.

718 19. Arfi Y, Minder L, Di Primo C, Le Roy A, Ebel C, Coquet L, et al. MIB-MIP is a
719 mycoplasma system that captures and cleaves immunoglobulin G. Proc Natl Acad Sci U S A.
720 2016;113(19):5406-11. doi: 10.1073/pnas.1600546113. PubMed PMID: 27114507; PubMed
721 Central PMCID: PMCPMC4868467.

722 20. Akarsu H, Bordes P, Mansour M, Bigot DJ, Genevaux P, Falquet L. TASmania: A
723 bacterial Toxin-Antitoxin Systems database. PLoS Comput Biol. 2019;15(4):e1006946. Epub
724 2019/04/26. doi: 10.1371/journal.pcbi.1006946. PubMed PMID: 31022176; PubMed Central
725 PMCID: PMCPMC6504116.

726 21. Hampton HG, Jackson SA, Fagerlund RD, Vogel AIM, Dy RL, Blower TR, et al.
727 AbiEi Binds Cooperatively to the Type IV abiE Toxin-Antitoxin Operator Via a Positively-
728 Charged Surface and Causes DNA Bending and Negative Autoregulation. J Mol Biol.
729 2018;430(8):1141-56. doi: 10.1016/j.jmb.2018.02.022. PubMed PMID: 29518409.

730 22. Gotfredsen M, Gerdes K. The Escherichia coli relBE genes belong to a new toxin-
731 antitoxin gene family. Molecular Microbiology. 1998;29(4):1065-76. doi: DOI
732 10.1046/j.1365-2958.1998.00993.x. PubMed PMID: WOS:000075451700013.

733 23. Yamamoto S, Kiyokawa K, Tanaka K, Moriguchi K, Suzuki K. Novel toxin-antitoxin
734 system composed of serine protease and AAA-ATPase homologues determines the high level

735 of stability and incompatibility of the tumor-inducing plasmid pTiC58. J Bacteriol.
736 2009;191(14):4656-66. Epub 2009/05/19. doi: 10.1128/JB.00124-09. PubMed PMID:
737 19447904; PubMed Central PMCID: PMCPMC2704731.

738 24. Zhang Y, Zhang J, Hoeflich KP, Ikura M, Qing G, Inouye M. MazF cleaves cellular
739 mRNAs specifically at ACA to block protein synthesis in Escherichia coli. Mol Cell.
740 2003;12(4):913-23. doi: 10.1016/s1097-2765(03)00402-7. PubMed PMID: 14580342.

741 25. UniProt C. UniProt: a worldwide hub of protein knowledge. Nucleic acids research.
742 2019;47(D1):D506-D15. doi: 10.1093/nar/gky1049. PubMed PMID: 30395287; PubMed
743 Central PMCID: PMCPMC6323992.

744 26. King KW, Dybvig K. Nucleotide sequence of *Mycoplasma mycoides* subspecies
745 *mycoides* plasmid pKMK1. Plasmid. 1992;28(1):86-91. Epub 1992/07/01. doi: 10.1016/0147-
746 619x(92)90039-d. PubMed PMID: 1518915.

747 27. Breton M, Tardy F, Dordet-Frisoni E, Sagne E, Mick V, Renaudin J, et al.
748 Distribution and diversity of mycoplasma plasmids: lessons from cryptic genetic elements.
749 BMC Microbiol. 2012;12:257. Epub 2012/11/14. doi: 10.1186/1471-2180-12-257. PubMed
750 PMID: 23145790; PubMed Central PMCID: PMCPMC3541243.

751 28. Leplae R, Geeraerts D, Hallez R, Guglielmini J, Dreze P, Van Melderen L. Diversity
752 of bacterial type II toxin-antitoxin systems: a comprehensive search and functional analysis
753 of novel families. Nucleic acids research. 2011;39(13):5513-25. Epub 2011/03/23. doi:
754 10.1093/nar/gkr131. PubMed PMID: 21422074; PubMed Central PMCID:
755 PMCPMC3141249.

29. Van Melderen L, Saavedra De Bast M. Bacterial toxin-antitoxin systems: more than selfish entities? PLoS Genet. 2009;5(3):e1000437. doi: 10.1371/journal.pgen.1000437. PubMed PMID: 19325885; PubMed Central PMCID: PMCPMC2654758.

30. Wen Y, Behiels E, Devreese B. Toxin-Antitoxin systems: their role in persistence, biofilm formation, and pathogenicity. Pathog Dis. 2014;70(3):240-9. doi: 10.1111/2049-632X.12145. PubMed PMID: 24478112.

31. Tandon H, Sharma A, Sandhya S, Srinivasan N, Singh R. *Mycobacterium tuberculosis* Rv0366c-Rv0367c encodes a non-canonical PezAT-like toxin-antitoxin pair. Sci Rep. 2019;9(1):1163. Epub 2019/02/06. doi: 10.1038/s41598-018-37473-y. PubMed PMID: 30718534; PubMed Central PMCID: PMCPMC6362051.

32. Akarsu H, Bordes P, Mansour M, Bigot D-J, Genevaux P, Falquet L. TASmania: A bacterial Toxin-Antitoxin Systems database. PLOS Computational Biology. 2019;15(4):e1006946. doi: 10.1371/journal.pcbi.1006946.

33. Fischer A, Shapiro B, Muriuki C, Heller M, Schnee C, Bongcam-Rudloff E, et al. The Origin of the '*Mycoplasma mycoides* Cluster' Coincides with Domestication of Ruminants. PLoS One. 2012;7(4):e36150. Epub 2012/05/05. doi: 10.1371/journal.pone.0036150. PubMed PMID: 22558362.

34. Thiaucourt F, Manso-Silvan L, Salah W, Barbe V, Vacherie B, Jacob D, et al. *Mycoplasma mycoides*, from "*mycoides* Small Colony" to "*capri*". A microevolutionary perspective. BMC Genomics. 2011;12:114. Epub 2011/02/18. doi: 10.1186/1471-2164-12-114. PubMed PMID: 21324191; PubMed Central PMCID: PMC3053259.

35. Sirand-Pugnet P, Lartigue C, Marenda M, Jacob D, Barre A, Barbe V, et al. Being pathogenic, plastic, and sexual while living with a nearly minimal bacterial genome. PLoS

779 Genet. 2007;3(5):e75. Epub 2007/05/22. doi: 10.1371/journal.pgen.0030075. PubMed PMID:
780 17511520; PubMed Central PMCID: PMCPMC1868952.

781 36. Sirand-Pugnet P, Citti C, Barre A, Blanchard A. Evolution of mollicutes: down a
782 bumpy road with twists and turns. Res Microbiol. 2007;158(10):754-66. Epub 2007/11/21.
783 doi: 10.1016/j.resmic.2007.09.007. PubMed PMID: 18023150.

784 37. Sevillano L, Diaz M, Yamaguchi Y, Inouye M, Santamaria RI. Identification of the
785 first functional toxin-antitoxin system in Streptomyces. PLoS One. 2012;7(3):e32977. doi:
786 10.1371/journal.pone.0032977. PubMed PMID: 22431991; PubMed Central PMCID:
787 PMCPMC3303803.

788 38. Huisman O, D'Ari R. An inducible DNA replication-cell division coupling
789 mechanism in E. coli. Nature. 1981;290(5809):797-9. doi: 10.1038/290797a0. PubMed
790 PMID: 7012641.

791 39. Justice SS, Hunstad DA, Cegelski L, Hultgren SJ. Morphological plasticity as a
792 bacterial survival strategy. Nat Rev Microbiol. 2008;6(2):162-8. doi: 10.1038/nrmicro1820.
793 PubMed PMID: WOS:000252426700015.

794 40. Harms A, Stanger FV, Scheu PD, de Jong IG, Goepfert A, Glatter T, et al.
795 Adenylylation of Gyrase and Topo IV by FicT Toxins Disrupts Bacterial DNA Topology.
796 Cell Rep. 2015;12(9):1497-507. Epub 2015/08/25. doi: 10.1016/j.celrep.2015.07.056.
797 PubMed PMID: 26299961.

798 41. Lartigue C, Vashee S, Algire MA, Chuang RY, Benders GA, Ma L, et al. Creating
799 bacterial strains from genomes that have been cloned and engineered in yeast. Science.
800 2009;325(5948):1693-6. Epub 2009/08/22. doi: 10.1126/science.1173759. PubMed PMID:
801 19696314.

802 42. Lartigue C, Valverde Timana Y, Labroussaa F, Schieck E, Liljander A, Sacchini F, et
803 al. Attenuation of a Pathogenic *Mycoplasma* Strain by Modification of the *obg* Gene by
804 Using Synthetic Biology Approaches. mSphere. 2019;4(3). doi: 10.1128/mSphere.00030-19.
805 PubMed PMID: 31118296.

806 43. Howe KL, Contreras-Moreira B, De Silva N, Maslen G, Akanni W, Allen J, et al.
807 Ensembl Genomes 2020-enabling non-vertebrate genomic research. Nucleic acids research.
808 2020;48(D1):D689-D95. Epub 2019/10/11. doi: 10.1093/nar/gkz890. PubMed PMID:
809 31598706; PubMed Central PMCID: PMCPMC6943047.

810 44. Salamov VSA, Solovyevand A. Automatic annotation of microbial genomes and
811 metagenomic sequences. Metagenomics and its applications in agriculture Nova Science
812 Publishers, Hauppauge. 2011:61-78.

813 45. Lartigue C, Blanchard A, Renaudin J, Thiaucourt F, Sirand-Pugnet P. Host specificity
814 of mollicutes oriC plasmids: functional analysis of replication origin. Nucleic acids research.
815 2003;31(22):6610-8. Epub 2003/11/07. doi: 10.1093/nar/gkg848. PubMed PMID: 14602921;
816 PubMed Central PMCID: PMCPMC275544.

817 46. Braga-Lagache S, Buchs N, Iacovache MI, Zuber B, Jackson CB, Heller M. Robust
818 Label-free, Quantitative Profiling of Circulating Plasma Microparticle (MP) Associated
819 Proteins. Mol Cell Proteomics. 2016;15(12):3640-52. Epub 2016/10/16. doi:
820 10.1074/mcp.M116.060491. PubMed PMID: 27738094; PubMed Central PMCID:
821 PMCPMC5141277.

822 47. Deutsch EW, Mendoza L, Shteynberg D, Farrah T, Lam H, Tasman N, et al. A guided
823 tour of the Trans-Proteomic Pipeline. Proteomics. 2010;10(6):1150-9. Epub 2010/01/27. doi:

824 10.1002/pmic.200900375. PubMed PMID: 20101611; PubMed Central PMCID:
825 PMCPMC3017125.

826 48. Eng JK, Hoopmann MR, Jahan TA, Egertson JD, Noble WS, MacCoss MJ. A deeper
827 look into Comet--implementation and features. J Am Soc Mass Spectrom. 2015;26(11):1865-
828 74. Epub 2015/06/28. doi: 10.1007/s13361-015-1179-x. PubMed PMID: 26115965; PubMed
829 Central PMCID: PMCPMC4607604.

830 49. Craig R, Beavis RC. A method for reducing the time required to match protein
831 sequences with tandem mass spectra. Rapid Commun Mass Spectrom. 2003;17(20):2310-6.
832 Epub 2003/10/15. doi: 10.1002/rcm.1198. PubMed PMID: 14558131.

833 50. Kim S, Pevzner PA. MS-GF+ makes progress towards a universal database search
834 tool for proteomics. Nat Commun. 2014;5:5277. Epub 2014/11/02. doi:
835 10.1038/ncomms6277. PubMed PMID: 25358478; PubMed Central PMCID:
836 PMCPMC5036525.

837 51. Tabb DL, Fernando CG, Chambers MC. MyriMatch: highly accurate tandem mass
838 spectral peptide identification by multivariate hypergeometric analysis. J Proteome Res.
839 2007;6(2):654-61. Epub 2007/02/03. doi: 10.1021/pr0604054. PubMed PMID: 17269722;
840 PubMed Central PMCID: PMCPMC2525619.

841 52. Choi H, Ghosh D, Nesvizhskii AI. Statistical validation of peptide identifications in
842 large-scale proteomics using the target-decoy database search strategy and flexible mixture
843 modeling. J Proteome Res. 2008;7(1):286-92. Epub 2007/12/15. doi: 10.1021/pr7006818.
844 PubMed PMID: 18078310.

845 53. Shteynberg D, Deutsch EW, Lam H, Eng JK, Sun Z, Tasman N, et al. iProphet: multi-
846 level integrative analysis of shotgun proteomic data improves peptide and protein

847 identification rates and error estimates. Mol Cell Proteomics. 2011;10(12):M111 007690.
848 Epub 2011/08/31. doi: 10.1074/mcp.M111.007690. PubMed PMID: 21876204; PubMed
849 Central PMCID: PMCPMC3237071.

850 54. Zybailov BL, Florens L, Washburn MP. Quantitative shotgun proteomics using a
851 protease with broad specificity and normalized spectral abundance factors. Mol Biosyst.
852 2007;3(5):354-60. Epub 2007/04/27. doi: 10.1039/b701483j. PubMed PMID: 17460794.

853 55. Zhang Y, Wen Z, Washburn MP, Florens L. Refinements to label free proteome
854 quantitation: how to deal with peptides shared by multiple proteins. Anal Chem.
855 2010;82(6):2272-81. Epub 2010/02/20. doi: 10.1021/ac9023999. PubMed PMID: 20166708.

856 56. Green MR, Sambrook J. Molecular cloning : a laboratory manual. 4th ed. Cold Spring
857 Harbor, N.Y.: Cold Spring Harbor Laboratory Press; 2012.

858 57. Schwendener S, Perreten V. The integrase of the Macrococcus caseolyticus resistance
859 island mecD (McRImecD) inserts DNA site-specifically into Staphylococcus and Bacillus
860 chromosomes. Mol Microbiol. 2018;110(3):455-68. doi: 10.1111/mmi.14112. PubMed
861 PMID: 30152907.

862 58. Dybvig K, Voelker LL. Molecular biology of mycoplasmas. Annu Rev Microbiol.
863 1996;50:25-57. doi: 10.1146/annurev.micro.50.1.25. PubMed PMID: 8905075.

864 59. Kolmogorov M, Yuan J, Lin Y, Pevzner PA. Assembly of long, error-prone reads
865 using repeat graphs. Nat Biotechnol. 2019;37(5):540-6. Epub 2019/04/03. doi:
866 10.1038/s41587-019-0072-8. PubMed PMID: 30936562.

867 60. Seemann T. Prokka: rapid prokaryotic genome annotation. Bioinformatics.
868 2014;30(14):2068-9. doi: 10.1093/bioinformatics/btu153. PubMed PMID: 24642063.

869 61. Darling AC, Mau B, Blattner FR, Perna NT. Mauve: multiple alignment of conserved
870 genomic sequence with rearrangements. Genome research. 2004;14(7):1394-403. doi:
871 10.1101/gr.2289704. PubMed PMID: 15231754; PubMed Central PMCID: PMC442156.

872 62. Kumar S, Stecher G, Li M, Knyaz C, Tamura K. MEGA X: Molecular Evolutionary
873 Genetics Analysis across Computing Platforms. Mol Biol Evol. 2018;35(6):1547-9. doi:
874 10.1093/molbev/msy096. PubMed PMID: 29722887; PubMed Central PMCID:
875 PMCPMC5967553.

876 63. Bertels F, Silander OK, Pachkov M, Rainey PB, van Nimwegen E. Automated
877 reconstruction of whole-genome phylogenies from short-sequence reads. Mol Biol Evol.
878 2014;31(5):1077-88. doi: 10.1093/molbev/msu088. PubMed PMID: 24600054; PubMed
879 Central PMCID: PMCPMC3995342.

880 64. Altschul SF, Gish W, Miller W, Myers EW, Lipman DJ. Basic local alignment search
881 tool. J Mol Biol. 1990;215(3):403-10. doi: 10.1016/S0022-2836(05)80360-2. PubMed PMID:
882 2231712.

883

884 **Tables**

885 **Table 1:** Candidate toxins and antitoxins of *M. mycoides* subsp. *capri* GM12 investigated in
886 this study. The top five candidate TAS were identified *in silico* by using the TASmania
887 database.

Name	Mnmemonic/ designation in manuscript	Size [nt/aa]	Gene annotation	Pfam/ predicted TAS type	E-value in TASmania
$TAS_{160/1}$	MMCAP2_0160 / T_{160}	753 /250	Abortive infection protein	AbiEii / IV	1.2e-53
	MMCAP2_0161 / A_{161}	597 /198	Abortive infection protein	AbiEi / IV	3.8e-49
$TAS_{889/0}$	MMCAP2_0889 / T_{889}	835 /278	Uncharacterized protein	AbiEii / IV	Guilty by association
	MMCAP2_0890 / A_{890}	600 /199	Conserved hypothetical protein	AbiEi / IV	2.6e-45
$TAS_{731/0}$	MMCAP2_0731 / T_{731}	1014 /337	Conserved hypothetical protein	AbiEii / IV	3.8e-29
	MMCAP2_0730 / A_{730}	600 /199	Conserved hypothetical protein	AbiEi / IV	Guilty by association
$TAS_{525/4}$	MMCAP2_0525 / T_{525}	402 /133	Hypothetical protein	MraZ / II	7e-26
	MMCAP2_0524 / A_{524}	927 /308	S-adenosyl-methyltransferase	MraW / II	Guilty by association
$TAS_{752/3}$	MMCAP2_0752 / T_{752}	573 /190	Cell filamentation protein	Fic / II	Guilty by association
	MMCAP2_0753 / A_{753}	273 /90	DNA-damage-inducible protein J	RelB / II	3.5e-9
$TAS_{133/2}$	MMCAP2_0133 / T_{133}	2274 /757	Subtilisin-like serine protease	- / II	N/A
	MMCAP2_0132 / A_{132}	1062 /353	AAA-ATPase	- / II	N/A

888 TAS: toxin-antitoxin system, T: toxin, A: antitoxin

889

Legends to Figures

Figure 1: Cartoon displaying the genomic localization and operon structure of candidate TAS of *M. mycoides* subsp. *capri* GM12

The circle displays the genome of GM12 (GenBank accession number: NZ_CP001668.1) including its GC content. Six candidate TAS operons are shown in boxes in relation to their localization in the genome. The promotor region, antitoxin and toxin are marked white, grey and black, respectively. Candidate TAS selected for functionality testing are highlighted with a red box.

Figure 2: Detection of proteomic signatures of TAS in *in vitro* grown GM12

The histogram shows relative protein abundance in strain GM12 [frequency over distributed normalized spectral abundance factor (dNSAF)], with candidate toxins (T) and antitoxins (A) marked as red arrows and the respective number of the toxin/antitoxin. Toxins and antitoxins had the following dNSAF values: A_{524} -3.47, T_{133} -3.92, A_{132} -3.92, A_{753} -3.92, A_{161} -4.45, T_{731} -4.52. Threshold values of "low, medium and high" expression levels are based on data distribution. Candidate toxins and antitoxins not displayed were below detection limits or absent.

Figure 3: Presence of six GM12 candidate TAS identified *in silico* in other mycoplasmas

Dots on the right indicate the presence of genes encoding candidate toxins or antitoxins. A) Phylogenetic tree based on whole genome sequences of different *M. mycoides* subsp. *capri* (*Mmc*) strains, *M. mycoides* subsp. *mycoides* (*Mmm*) strain $PG1^T$ was used as outgroup. The tree was constructed using Neighbor-joining inference method, evolutionary distance was calculated using Maximum Composite Likelihood method with rate variation among site

915 modelled with a gamma distribution. Bootstrap values (100 replicates) are displayed next to
916 tree branches. B) Phylogenetic tree of different members of the '*M. mycoides* cluster' based on
917 16S rRNA sequences, *M. putrefaciens* strain KS1^T was used as outgroup. The tree was
918 constructed using Neighbor-joining inference method. Bootstrap values (100 replicates) are
919 displayed next to tree branches.
920
921 **Figure 4: Toxicity of recombinant T_{133} on *E. coli* LMG194**
922 A) Growth curves of *E. coli* LMG194 in response to induction or repression of heterologous
923 expression of T_{133} and empty vector pBAD/His. Each data point represents the mean of three
924 biological replicates, bars indicate standard deviation. The p-values are displayed (* $p \leq 0.05$,
925 ** $p \leq 0.01$). B) Scanning electron micrograph (magnification 10,000x) displaying
926 morphological changes of *E. coli* LMG194 after heterologous expression of T_{133}. Blebbing at
927 the pole is indicated by an arrow, z-shaped cells by asterisk and cell debris by arrowheads.
928
929 **Figure 5: Toxicity of recombinant T_{752} on *B. subtilis* 168 Marburg**
930 A) Growth curves of *B. subtilis* 168 Marburg in response to induction of heterologous
931 expression of T_{752} andstrain 168 Marburg. Each data point represents the mean of three
932 biological replicates, bars indicate standard deviation. The p-values are displayed (* $p \leq 0.05$,
933 ** $p \leq 0.01$ and *** $p \leq 0.001$). B) Scanning electron micrograph (magnification 10,000x)
934 displaying morphological changes of *B. subtilis* 168 Marburg after induction of heterologous
935 expression. Indentations of cells are indicated by asterisk, empty/ shrunk cells by arrowhead
936 and shrunk cells upon division by arrows.
937
938 **Figure 6: Effect of cloned toxins, antitoxins and TAS on the transformation rate into *M.***
939 ***capricolum* subsp. *capricolum***

940 *M. capricolum* subsp. *capricolum* ATCC 27343^{T} was transformed with different plasmid
941 constructs harboring either entire TAS operons ($TAS_{133/2}$, $TAS_{752/3}$ and $TAS_{160/1}$), individual
942 toxins or antitoxins. Empty pMYCO1 plasmid was used as a positive control. Each column
943 represents the mean of three independent biological replicates and bars indicate standard
944 deviations. Significance is indicated (** $p \leq 0.01$, *** $p \leq 0.001$, **** $p \leq 0.0001$).

945 **Supporting information**

946 **Figure S1: Detection of transcripts of candidate TAS**

947 PCR using cDNA as template was used to detect transcripts. Amplicons have been separated
948 using a 1% agarose gel. Gels on the left show amplicons obtained using gDNA as template.
949 The gels on the right show amplicons obtained using cDNA as template and therefore presence
950 of transcripts. Complementary DNA (cDNA) was synthesized by RT-PCR using RNA of
951 GM12 as template. M: 1 kbp GeneRuler DNA ladder.

952

953 **Figure S2: MAUVE alignment of 16 *Mmc* genomes**

954 Multiple sequence alignment of different *M. mycoides* subsp. *capri* genomes using Progressive
955 MAUVE and default parameters. Colored blocks are collinear and homologous regions.
956 Inversions of colinear blocks are displayed below the centre line of the genome. Strain names
957 are marked at the left of each alignment block and positions on the genomes are marked on top.

958

959 **Figure S3: Heterologous expression of different candidate toxins and antitoxins in *E. coli***

960 A) Immunoblot analysis of *E. coli* expressing heterologous candidate toxins and antitoxins
961 cloned into the pBAD/His expression vector. Expression was induced by addition of arabinose.
962 Expression was monitored over 7 h. 100 µg total protein was separated onto a 12% SDS PAGE
963 before being transferred to a nitrocellulose membrane. PageRuler™ was used as size marker.
964 B) Growth curves of *E. coli* harboring candidate toxins T_{752}, T_{160} or antitoxins A_{753}, A_{161} or
965 A_{132} upon induction (solid line) or repression of expression (dashed line). C) Scanning electron
966 micrographs (magnification 10,000x) displaying *E. coli* harboring pBAD/His constructs with
967 toxin T_{133}, antitoxin A_{132} or empty vector pBAD/His either induced with arabinose or repressed
968 with glucose.

969

Figure S4: Heterologous expression of different candidate toxins and antitoxins in *B. subtilis*

A) Growth curves of *B. subtilis* harboring candidate antitoxin A_{161}, toxin T_{160} or 168 Marburg with (solid line) and without (dashed line) induction of expression. B) Scanning electron micrographs (magnification 10,000x) displaying *B. subtilis* harboring pHT01 constructs with antitoxin A_{161}, toxin T_{160}, or empty vector pHT01 either induced with IPTG or uninduced.

Table S1: TASmania database output file for *M. mycoides* subsp. *capri* GM12

Table S2: Output list of proteome analysis of *M. mycoides* subsp. *capri* GM12

Table S3: *M. mycoides* subsp. *capri* strains sequenced in this study

Table S4: TBLASTN results for candidate TAS presence in different *M. mycoides* subsp. *capri* strains and different other mycoplasmas

Table S5: Oligonucleotide primers used in this study

File S1: Plasmids constructed in this study and codon-optimized toxin and antitoxin encoding genes cloned for heterologous expression as well as TAS nucleotide sequences cloned into pMYCO1.

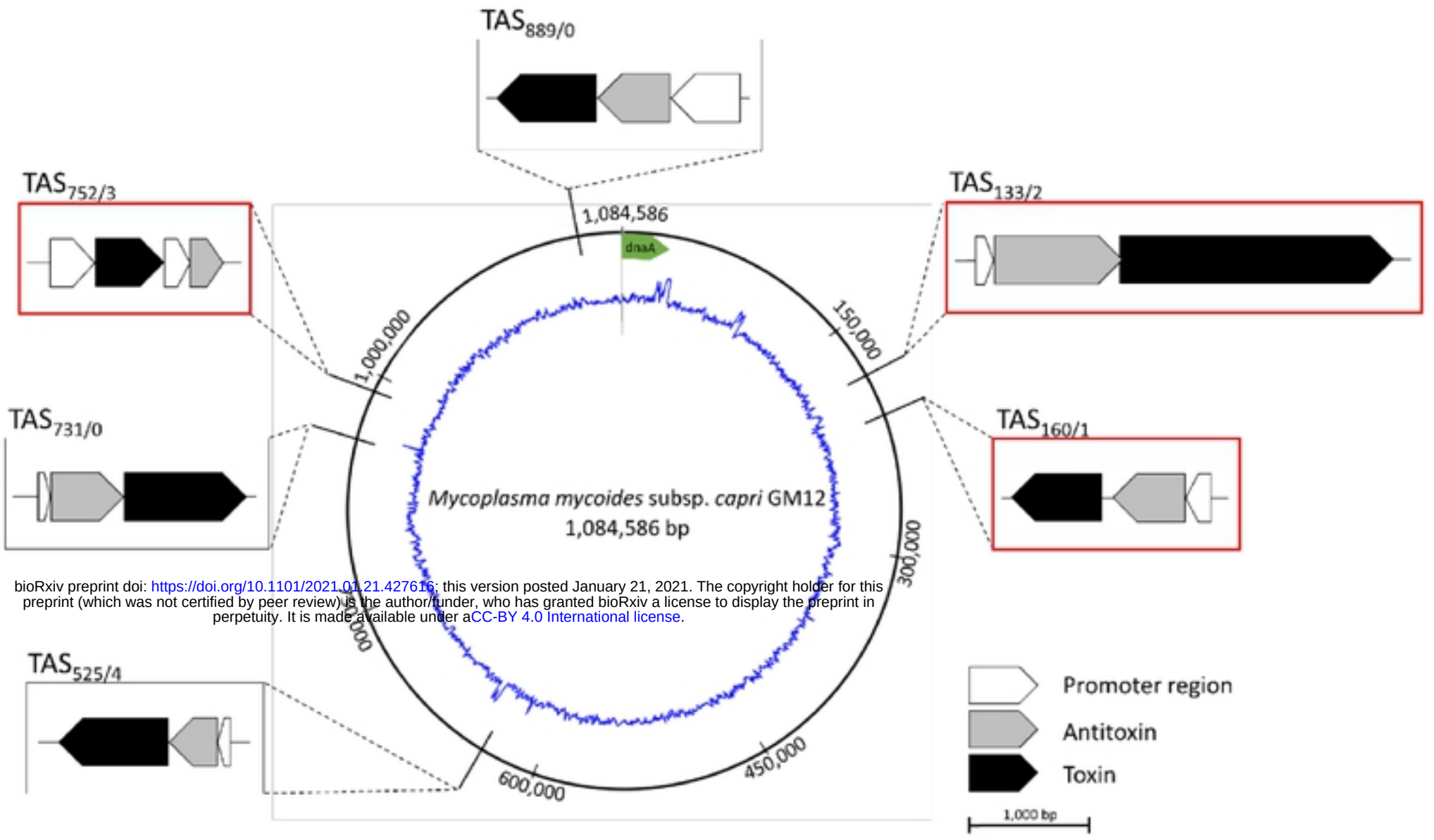

Figure 1: Cartoon displaying the genomic localization and operon structure of candidate TAS of M. mycoides subsp. capri GM12

The circle displays the genome of GM12 (GenBank accession number: NZ_CP001668.1) including its GC content. Six candidate TAS operons are shown in boxes in relation to their localization in the genome. The promotor region, antitoxin and toxin are marked white, grey and black, respectively. Candidate TAS selected for functionality testing are highlighted with a red box.

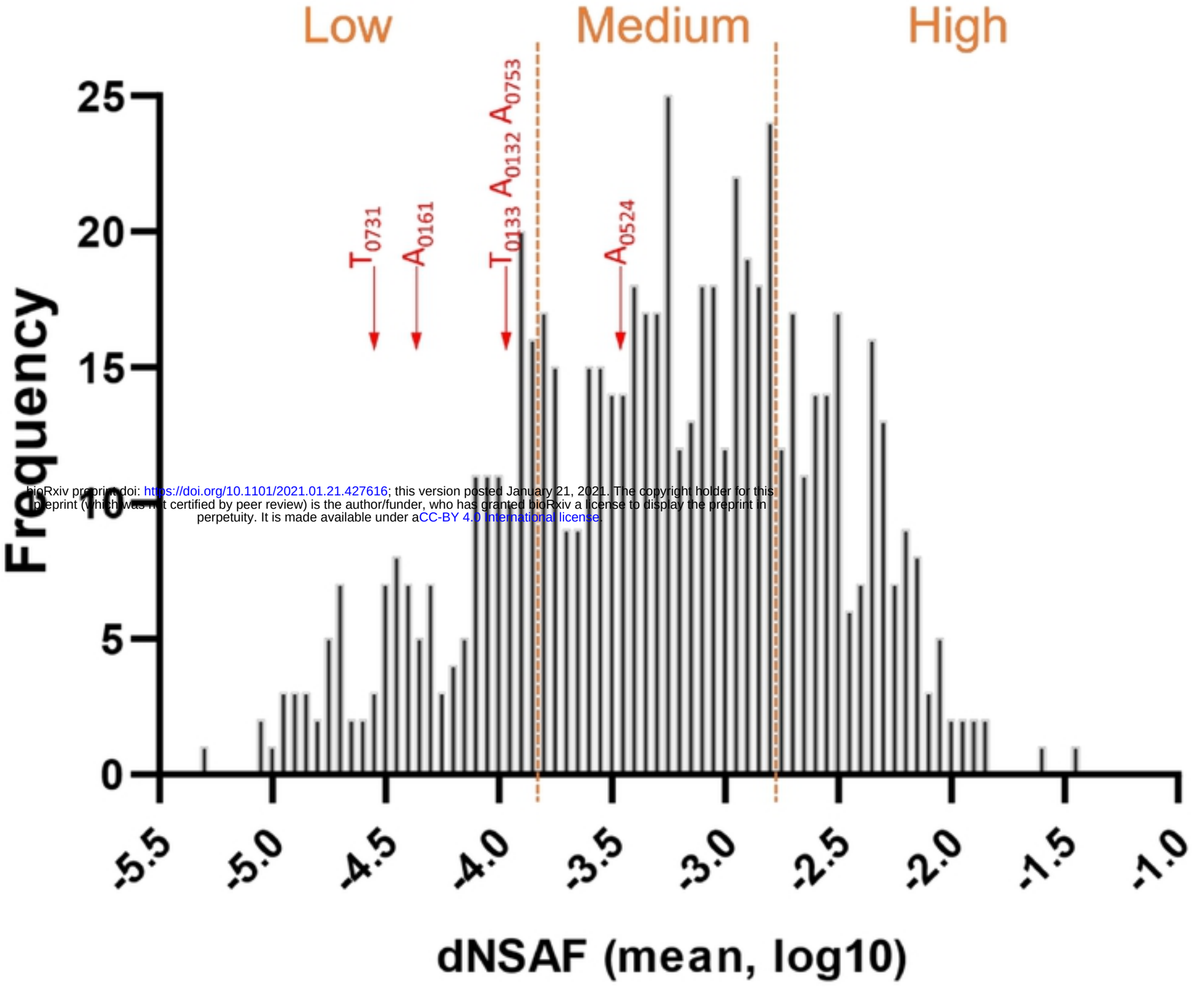

Figure 2: Detection of proteomic signatures of TAS in in vitro grown GM12

The histogram shows relative protein abundance in strain GM12 [frequency over distributed normalized spectral abundance factor (dNSAF)], with candidate toxins (T) and antitoxins (A) marked as red arrows and the respective number of the toxin/antitoxin. Toxins and antitoxins had the following dNSAF values: A_{524} -3.47, T_{133} -3.92, A_{132} -3.92, A_{753} -3.92, A_{161} -4.45, T_{731} -4.52. Threshold values of "low, medium and high" expression levels are based on data distribution. Candidate toxins and antitoxins not displayed were below detection limits or absent.

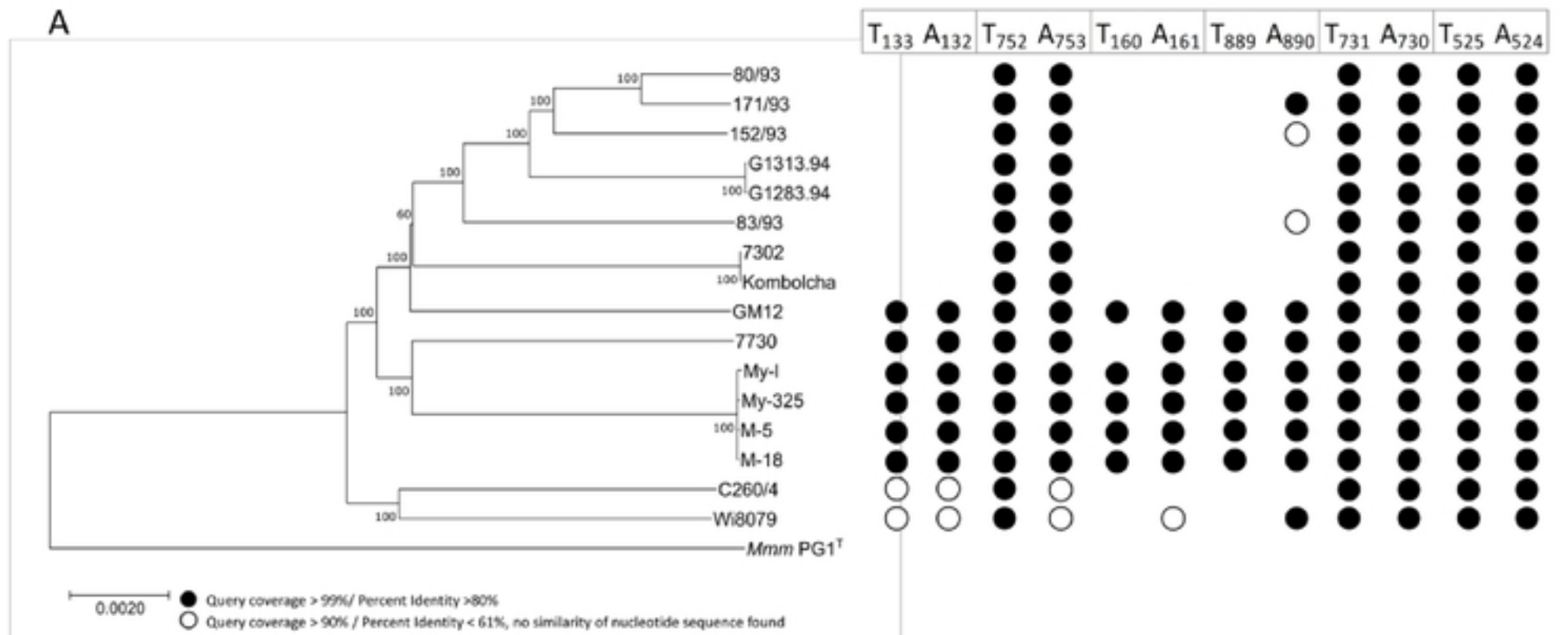

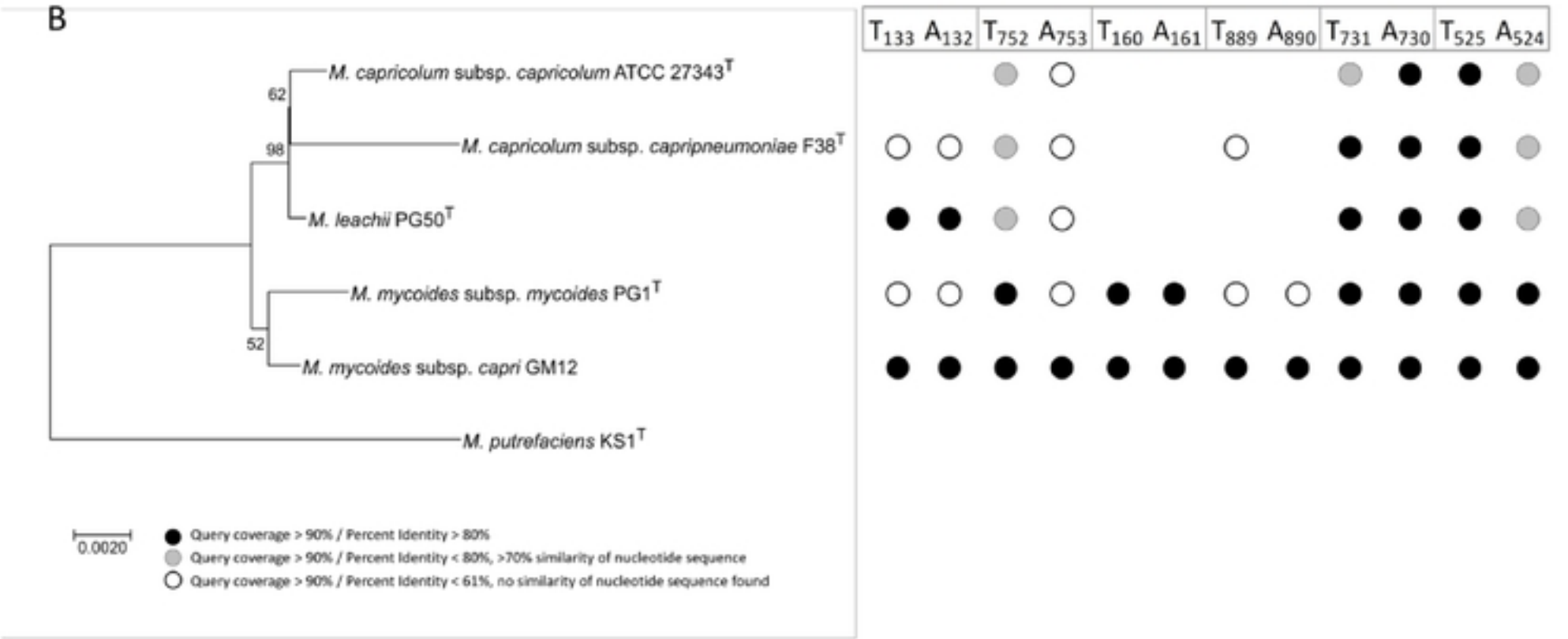

Figure 3: Presence of six GM12 candidate TAS identified in silico in other mycoplasmas

Dots on the right indicate the presence of genes encoding candidate toxins or antitoxins. A) Phylogenetic tree based on whole genome sequences of different M. mycoides subsp. capri (Mmc) strains, M. mycoides subsp. mycoides (Mmm) strain PG1^T was used as outgroup. The tree was constructed using Neighbor-joining inference method, evolutionary distance was calculated using Maximum Composite Likelihood method with rate variation among site modelled with a gamma distribution. Bootstrap values (100 replicates) are displayed next to tree branches. B) Phylogenetic tree based on 16S rRNA sequences of different members of the 'M. mycoides cluster', M. putrefaciens strain KS1 was used as outgroup. The tree was constructed using Neighbor-joining inference method. Bootstrap values (100 replicates) are displayed next to tree branches.

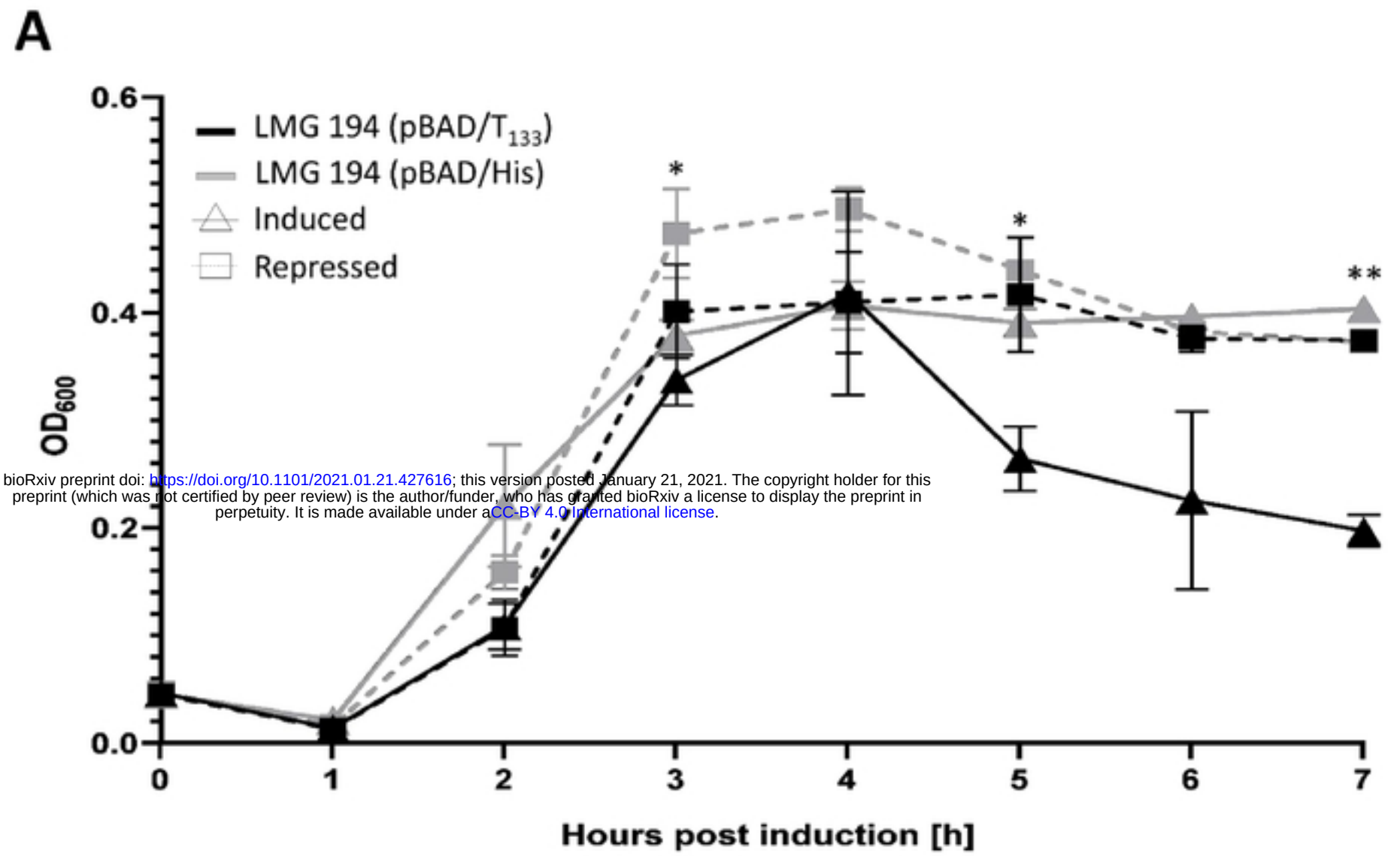

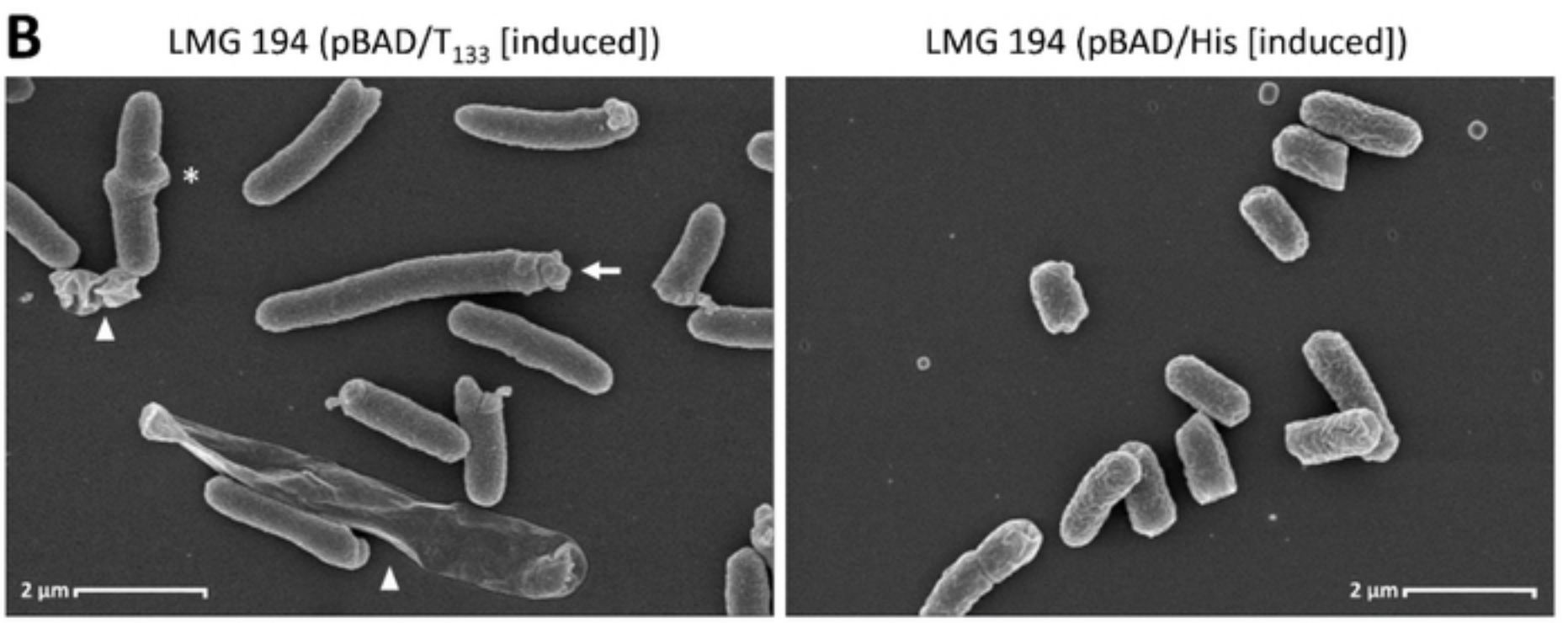

Figure 4: Toxicity of recombinant T_{133} on E. coli LMG 194

A) Growth curves of E. coli LMG 194 in response to induction or repression of heterologous expression of T_{133} and empty vector pBAD/His. Each data point represents the mean of three biological replicates, bars indicate standard deviation. The p-values are displayed (* $p \leq 0.05$, ** $p \leq 0.01$). B) Scanning electron micrograph (magnification 10,000x) displaying morphological changes of E. coli LMG 194 after heterologous expression of T_{133}. Blebbing at the pole is indicated by an arrow, z-shaped cells by asterisk and cell debris by arrowheads.

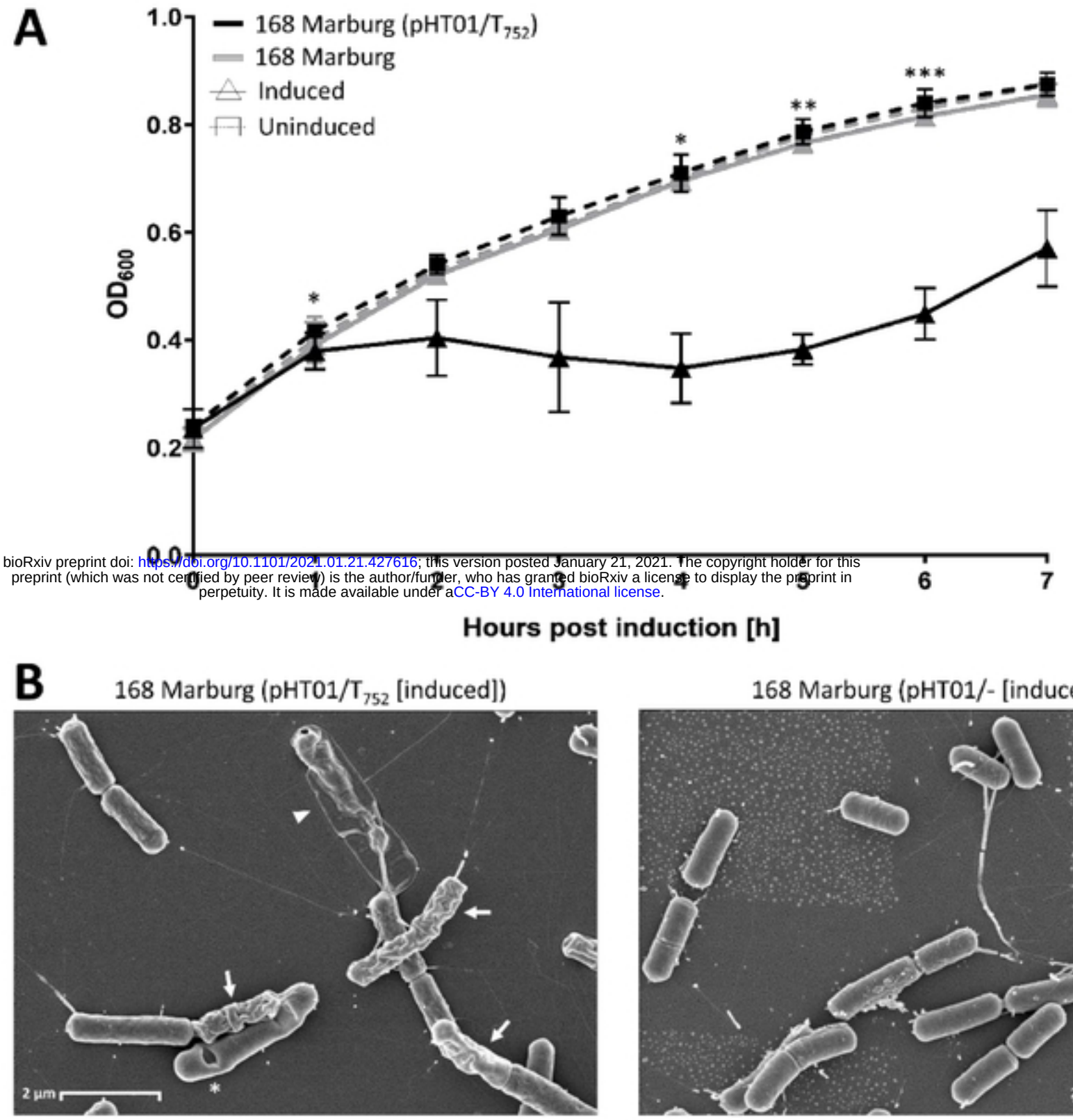

Figure 5: Toxicity of recombinant T_{752} on B. subtilis 168 Marburg

A) Growth curves of B. subtilis 168 Marburg in response to induction of heterologous expression of T_{752} andstrain 168 Marburg. Each data point represents the mean of three biological replicates, bars indicate standard deviation. The p-values are displayed (* $p \leq 0.05$, ** $p \leq 0.01$ and *** $p \leq 0.001$). B) Scanning electron micrograph (magnification 10,000x) displaying morphological changes of B. subtilis 168 Marburg after induction of heterologous expression. Indentations of cells are indicated by asterisk, empty/ shrunk cells by arrowhead and shrunk cells upon division by arrows.

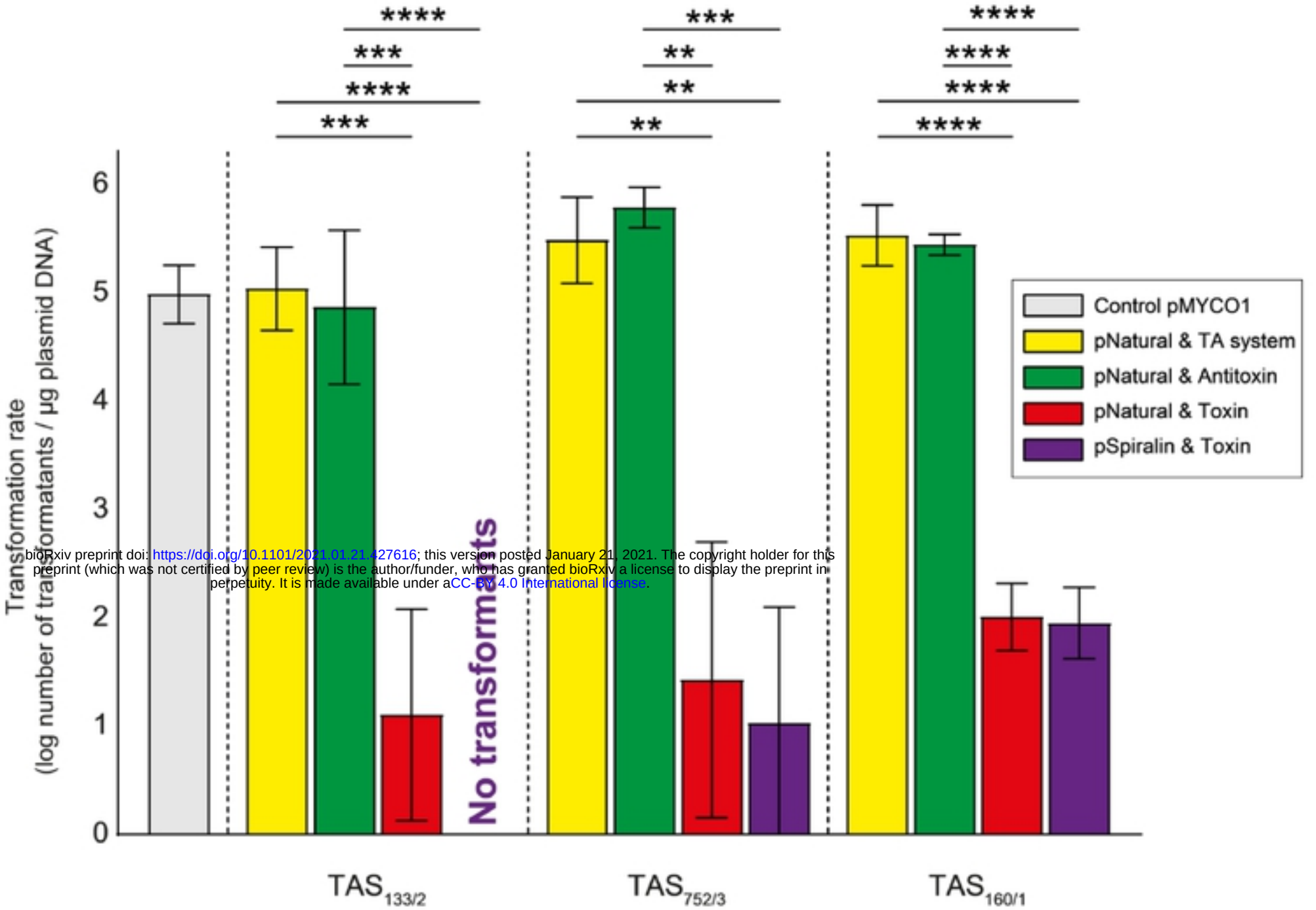

Figure 6: Effect of cloned toxins, antitoxins and TAS on the transformation rate into M. capricolum subsp. capricolum

M. capricolum subsp. capricolum ATCC 27343^T was transformed with different plasmid constructs harboring either entire TAS operons ($TAS_{133/2}$, $TAS_{752/3}$ and $TAS_{160/1}$), individual toxins or antitoxins. Empty pMYCO1 plasmid was used as a positive control. Each column represents the mean of three independent biological replicates and bars indicate standard deviations. Significance is indicated (** $p \leq 0.01$, *** $p \leq 0.001$, **** $p \leq 0.0001$).